Aqueous-phase reactive species formed by fine particulate matter from remote forests and polluted urban air

Haijie Tong[1,2*], Fobang Liu[1,3], Alexander Filippi[1], Jake Wilson[1], Andrea M. Arangio[1,4], Yun Zhang[5], Siyao Yue[6,7,8], Steven Lelieveld[1], Fangxia Shen[1,9], Helmi-Marja K. Keskinen[10,11], Jing Li[12], Haoxuan Chen[12], Ting Zhang[12], Thorsten Hoffmann[5], Pingqing Fu[8], William H. Brune[13], Tuukka Petäjä[10], Markku Kulmala[10], Maosheng Yao[12], Thomas Berkemeier[1], Manabu Shiraiwa[14], Ulrich Pöschl[1]

[1] Multiphase Chemistry Department, Max Planck Institute for Chemistry, 55128 Mainz, Germany
[2] Now at: Department of Civil and Environmental Engineering, The Hong Kong Polytechnic University, Kowloon, Hong Kong, China
[3] School of Chemical and Biomolecular Engineering, Georgia Institute of Technology, Atlanta, Georgia 30332, USA
[4] École Polytechnique Fédérale de Lausanne, Lausanne 1015, Switzerland
[5] Institute of Inorganic and Analytical Chemistry, Johannes Gutenberg University, 55128 Mainz, Germany
[6] State Key Laboratory of Atmospheric Boundary Layer Physics and Atmospheric Chemistry, Institute of Atmospheric Physics, Chinese Academy of Sciences, Beijing, 100029, China
[7] College of Earth and Planetary Sciences, University of Chinese Academy of Sciences, Beijing, 100049, China
[8] Institute of Surface-Earth System Science, Tianjin University, Tianjin, 300072, China
[9] School of Space and Environment, Beihang University, Beijing, 100191, China
[10] Institute for Atmospheric and Earth System Research / Physics, Faculty of Science, University of Helsinki, P.O. Box 64, FIN-00014, Helsinki, Finland
[11] Hyytiälä Forestry Field Station, Hyytiäläntie 124, FI-35500 Korkeakoski, Finland
[12] College of Environmental Sciences and Engineering, Peking University, Beijing, 100871, China
[13] Department of Meteorology, Pennsylvania State University, University Park, Pennsylvania 16802, USA
[14] Department of Chemistry, University of California, Irvine, California 92697-2025, USA

Correspondence to: Haijie Tong (h.tong@mpic.de; haijie.tong@polyu.edu.hk)

Abstract

In the aqueous phase, fine particulate matter can form reactive species (RS) that influence the aging, properties, and health effects of atmospheric aerosols. In this study, we explore the RS yields of aerosol samples from remote forest (Hyytiälä, Finland) and polluted urban locations (Mainz, Germany; Beijing, China), and we relate the RS yields to different chemical constituents and reaction mechanisms. Ultrahigh-resolution mass spectrometry was used to characterize organic aerosol composition, electron paramagnetic resonance (EPR) spectroscopy with a spin-trapping technique was applied to determine the concentrations of $^{\bullet}OH$, $O_2^{\bullet-}$, and carbon- or oxygen-centered organic radicals, and a fluorometric assay was used to quantify H_2O_2. The aqueous H_2O_2-forming potential per mass unit of ambient $PM_{2.5}$ (particle diameter < 2.5 µm) was roughly the same for all investigated samples, whereas the mass-specific yields of radicals were lower for sampling sites with higher concentration of $PM_{2.5}$. The abundances of water-soluble transition metals and aromatics in ambient $PM_{2.5}$ were positively correlated with the relative fraction of $^{\bullet}OH$ and negatively correlated with the relative fraction of carbon-centered radicals. In contrast, highly oxygenated organic molecules (HOM) were positively correlated with the relative fraction of carbon-centered radicals and negatively correlated with the relative fraction of $^{\bullet}OH$. Moreover, we found that the relative fractions of different types of radicals formed by ambient $PM_{2.5}$ were comparable to surrogate mixtures comprising transition metal ions, organic hydroperoxide, H_2O_2, and humic or fulvic acids. The interplay of transition metal ions (e.g., iron and copper ions), highly oxidized organic molecules (e.g., hydroperoxides), and complexing or scavenging agents (e.g., humic or fulvic acids), leads to non-linear concentration dependencies in the aqueous-phase RS production. A strong dependence on chemical composition was also observed for the aqueous-phase radical yields of laboratory-generated secondary organic aerosols (SOA) from precursor mixtures of naphthalene and β-pinene. Our findings show how the composition of $PM_{2.5}$ can influence the amount and nature of aqueous-phase RS, which may explain differences in the chemical reactivity and health effects of particulate matter in clean and polluted air.

1 Introduction

Atmospheric fine particulate matter with a particle diameter < 2.5 µm ($PM_{2.5}$) can form reactive species (RS) upon dissolution in the aqueous phase (Bates et al., 2015;Lakey et al., 2016;Park et al., 2018;Li et al., 2018;Tong et al., 2019). The umbrella term RS comprises reactive oxygen species (e.g., $^\bullet OH$, $O_2^{\bullet-}$, $^1O_2$, H_2O_2, and ROOH) as well as C- and O-centered organic radicals (Halliwell and Whiteman, 2004;Sies et al., 2017), which influence the chemical aging of atmospheric aerosols and their interaction with the biosphere (Pöschl and Shiraiwa, 2015;Reinmuth-Selzle et al., 2017;Shiraiwa et al., 2017). For example, Fenton-like reactions of hydroperoxides with transition metal ions contribute to the formation of aqueous-phase radicals including $^\bullet OH$ (Jacob, 2000;Enami et al., 2014;Anglada et al., 2015;Tong et al., 2016a), enhancing the conversion of organic precursors to secondary organic aerosols (SOA) (Donaldson and Valsaraj, 2010;Ervens et al., 2011;Gligorovski et al., 2015;Gilardoni et al., 2016). Moreover, $PM_{2.5}$ may generate excess concentrations of RS in human airways, causing antioxidant depletion, oxidative stress, and respiratory diseases (Nel, 2005;Cui et al., 2015;Lakey et al., 2016;Qu et al., 2017;Lelieveld and Pöschl, 2017;Rao et al., 2018).

The formation pathways and yields of RS from ambient PM and laboratory-generated SOA have been investigated in a wide range of studies (Valavanidis et al., 2005;Ohyama et al., 2007;Chen et al., 2010;Wang et al., 2011a;Wang et al., 2011b;Verma et al., 2014;Badali et al., 2015;Bates et al., 2015;Verma et al., 2015;Arangio et al., 2016;Tong et al., 2016a;Kuang et al., 2017;Tong et al., 2017;Zhou et al., 2018;Tong et al., 2019;Chowdhury et al., 2019;Fang et al., 2019;Liu et al., 2020). The mass, surface area, and chemical composition of PM were discussed as key factors influencing the reactivity of atmospheric aerosols (Møller et al., 2010;Fang et al., 2015;Jin et al., 2019;Lammel et al., 2020). Among the substance groups associated with RS formation by PM in water are black carbon (Baumgartner et al., 2014), transition metals (Yu et al., 2018), oxidized aromatic compounds including quinones and environmentally persistent free radicals (EPFR) (Xia et al., 2004;Gehling et al., 2014;Charrier et al., 2014;Xiong et al., 2017), humic-like substances (HULIS) (Lin and Yu, 2011;Page et al., 2012;Fang et al., 2019), and peroxide-containing highly oxygenated

77 organic molecules (HOM) (Chen et al., 2010;Wang et al., 2011b;Tong et al., 2016a;Tong et al., 2018;Tong

78 et al., 2019;Fang et al., 2020;Qiu et al., 2020). Moreover, the HULIS and other multifunctional compounds

79 containing carboxyl, carboxylate, phenolic, and quinoid groups may influence the redox activity of PM via

80 chelating transition metals (Laglera and van den Berg, 2009;Kostić et al., 2011;Catrouillet et al.,

81 2014;Gonzalez et al., 2017;Wang et al., 2018c;Win et al., 2018;Wei et al., 2019).

82 To assess the oxidative potential of ambient PM, the following cellular or acellular assays have been

83 used: dichloro-dihydro-fluorescein diacetate (DCFH-DA), dithiothreitol (DTT), ascorbic acid (AA),

84 macrophage, electron paramagnetic resonance (EPR), and surrogate lung fluids (SLF) (Landreman et al.,

85 2008;Charrier and Anastasio, 2012;Kalyanaraman et al., 2012;Charrier et al., 2014;Charrier and Anastasio,

86 2015;Fang et al., 2016;Tong et al., 2018;Bates et al., 2019;Fang et al., 2019;Molina et al., 2020;Crobeddu

87 et al., 2020). However, the interplay of different PM constituents often results in non-additive

88 characteristics of the RS yields or oxidative potential of PM (Charrier et al., 2014;Lakey et al., 2016;Wang

89 et al., 2018b). Thus, unraveling the adverse health effects of ambient PM requires systematic investigations

90 of the RS formation and chemical reactivity of PM from different sources and environments (Shiraiwa et

91 al., 2017).

92 The concentration of $PM_{2.5}$ and the composition of airborne organic matter vary considerably from clean

93 forest to polluted urban environments. For example, the $PM_{2.5}$ concentrations at the Hyytiälä forest site are

94 typically below 10 µg m^{-3}, with organic matter accounting for ~70% (Laakso et al., 2003;Maenhaut et al.,

95 2011), whereas the $PM_{2.5}$ concentrations in Beijing during winter can reach and exceed daily average values

96 of 150 µg m^{-3}, with organic matter accounting for ~40% (Huang et al., 2014). Moreover, anthropogenic

97 emissions can enhance the formation of biogenic SOA and HOM as well as the levels of particulate

98 transition metals, humic-like substances, and PM oxidative potential (Goldstein et al., 2009;Hoyle et al.,

99 2011;Liu et al., 2014;Xu et al., 2015;Ma et al., 2018;Pye et al., 2019;Shrivastava et al., 2019).

100 In this study, we compared the RS yields of $PM_{2.5}$ in clean and polluted environments. We used three

101 approaches to explore the RS formation by $PM_{2.5}$ from remote forest of Hyytiälä (Finland), intermediately

102 polluted city of Mainz (Germany), and heavily polluted megacity of Beijing (China) (Figure 1). To quantify

103 the abundances of redox-active PM constituents related to RS formation, we collected ambient $PM_{2.5}$ and

104 measured the chemical composition of organic matter, the abundance of water-soluble transition metals,

105 and the yield of radicals and H_2O_2 in the liquid phase (Figure 1a). To assess the influence of anthropogenic-

106 biogenic organic matter interactions on the RS formation by ambient $PM_{2.5}$, we analyzed the radical yield

107 of SOA generated by oxidation of mixed anthropogenic and biogenic precursors in a laboratory chamber

108 (Figure 1b). To gain insights into the radical formation mechanism of ambient $PM_{2.5}$ in water, we

109 differentiated the influence of transition metal ions, organic hydroperoxide (ROOH), water-soluble humic

110 acid (HA) and fulvic acid (FA) on the radical formation by Fenton-like reactions (Figure 1c).

2 Materials and methods

2.1 Chemicals

113 The following chemicals were used as received without further purification: β-pinene (99%, Sigma-

114 Aldrich), naphthalene (99.6%, Alfa Aesar GmbH&Co KG), cumene hydroperoxide (80%, Sigma-Aldrich),

115 H_2O_2 (30%, Sigma-Aldrich), $FeSO_4 \cdot 7H_2O$ (F7002, Sigma-Aldrich), $CuSO_4 \cdot 5H_2O$ (209198, Sigma-

116 Aldrich), $NiCl_2$ (98%, Sigma-Aldrich), $MnCl_2$ (≥ 99%, Sigma-Aldrich), VCl_2 (85%, Sigma-Aldrich), NaCl

117 (443824T, VWR International GmbH), KH_2PO_4 (≥ 99%, Alfa Aesar GmbH&Co KG), Na_2HPO_4 (≥

118 99.999%, Fluka), humic acid (53680, Sigma-Aldrich), fulvic acid (AG-CN2-0135-M005, Adipogen), 5-

119 tert-Butoxycarbonyl-5-methyl-1-pyrroline-N-oxide (BMPO, high purity, Enzo Life Sciences, Inc.), H_2O_2

120 assay kit (MAK165, Sigma-Aldrich), ultra-pure water (14211-1L-F, Sigma-Aldrich), 47 mm diameter

121 Teflon filters (JVWP04700, Omnipore membrane filter), and micropipettes (50 µL, Brand GmbH&Co KG).

122 The used neutral saline (pH=7.4) consists of 10 mM phosphate buffer (2.2 mM KH_2PO_4 and 7.8 mM

123 Na_2HPO_4) and 114 mM NaCl, which was used to simulate physiologically relevant condition.

2.2 Collection and extraction of ambient fine PM

125 Ambient fine particles were collected onto Teflon filters for all sites. The Hyytiälä $PM_{2.5}$ was collected

126 using a three-stage cascade impactor (Dekati® PM10) at the Station for Measuring Forest Ecosystem-

127 Atmosphere Relations station (SMEAR II station, Finland) during 31 May-19 July 2017 (Hari and Kulmala,

128   2005). The Mainz fine PM was collected using a micro-orifice uniform deposit impactor (MOUDI, 122-R,

129   MSP Corporation) (Arangio et al., 2016) on the roof of the Max Planck Institute for Chemistry during 22

130   August-17 November 2017 and 23-31 August 2018. The Beijing winter $PM_{2.5}$ was collected using a 4-

131   channel $PM_{2.5}$ air sampler (TH-16, Wuhan Tianhong Instruments Co., Ltd.) in the campus of the Peking

132   University, an urban site of Beijing, during 20 December-13 January 2016 and 6 November-17 January

133   2018 (Lin et al., 2015). The sampling time for a single filter sample in Hyytiälä, Mainz, and Beijing are 48-

134   72, 25-54, and 5-24 h, respectively, depending on the local PM concentrations. More information about the

135   sampling is shown in Table S1. After sampling, all filter samples were put in petri dishes and stored in a -

136   80 ℃ freezer before analysis. To determine the mass of collected PM, each filter was weighed before and

137   after the collection using a high sensitivity balance (±10 µg, Mettler Toledo XSE105DU). In Hyytiälä, the

138   PM_1 and $PM_{1-2.5}$ were separately sampled, which were combined and extracted together to represent $PM_{2.5}$

139   samples. Mainz PM with cut-size range of 0.056-1.8 µm is taken as a proxy for $PM_{2.5}$. Particle

140   concentrations in aqueous extracts were estimated to be in the range of 200-6000 µg mL^{-1} (Figure S1).

141   **2.3 Formation, collection, and extraction of laboratory-generated SOA**

142   To generate SOA from mixed anthropogenic and biogenic precursors, different concentrations of gas-phase

143   naphthalene and β-pinene were mixed and oxidized in a potential aerosol mass (PAM) chamber, i.e., an

144   oxidation flow reactor (OFR) (Kang et al., 2007;Tong et al., 2018). Naphthalene and β-pinene were used

145   as representative SOA precursors in Beijing and Hyytiälä, respectively (Hakola et al., 2012;Huang et al.,

146   2019). The concentrations of gas-phase O_3 and $^{\bullet}OH$ in the PAM chamber were ~1 ppm and ~5.0×10^{11} cm-

147   ^{3} (Tong et al., 2018), respectively. SOA was produced by adjusting the relative concentrations of

148   naphthalene to the sum of it with β-pinene (i.e., [naphthalene]/([naphthalene] + [β-pinene])) to be ~9%,

149   ~23%, and ~38% (mass fraction), respectively. The concentrations of naphthalene and β-pinene were 0.2-

150   0.6 ppm and 1.0-2.5 ppm, respectively, which were determined on the basis of a calibration function

151   measured by gas chromatography mass spectrometry (Tong et al., 2018). The number and size distributions

152   of SOA particles were meaured using a scanning mobility particle sizer (SMPS, GRIMM Aerosol Technik

153 GmbH&Co. KG). When the SOA concentration was stable, 47 mm diameter Teflon filters (JVWP04700,

154 Omnipore membrane filter) were used to collect SOA particles, which were extracted into water solutions

155 within 2 minutes after the sampling. More information about the SOA formation, characterization,

156 collection, and extraction can be found in previous studies (Tong et al., 2016a;Tong et al., 2017;Tong et al.,

157 2018;Tong et al., 2019).

158 2.4 Surrogate mixtures

159 We used cumene hydroperoxide (CHP), humic acid (HA), fulvic acid (FA), and H_2O_2 as model compounds

160 mimicking the redox-active substances in ambient particulate matter (Lin and Yu, 2011;Ma et al.,

161 2018;Tong et al., 2019). The following method was used to prepare HA or FA solutions. First, 0-1000 µg

162 mL^{-1} HA or FA water suspensions were made. Then, the suspensions were sonicated for 3 minutes to

163 accelerate the dissolution of HA or FA. Afterwards, the sonicated suspensions were centrifuged at 6000

164 rpm (MiniStar, VWR International bvba) for 2 minutes. Finally, the supernatants were taken out from the

165 centrifuge tubes with pipettes and stored in glass vials under 4-8 °C condition before analysis. The HA or

166 FA solutions were prepared freshly day-to-day. To determine the concentrations of dissolved HA or FA,

167 aliquots of the supernatants were dried with pure N_2 flow (1-2 bar) and weighted with a high sensitivity

168 balance (± 0.01 mg, Mettler Toledo XSE105DU). The concentrations of Fe^{2+}, Cu^{2+}, HA, and H_2O_2 in the

169 surrogate mixtures are 43 µM, 3 µM, 4 mg L^{-1}, and 7 µM, which are based on the measurement of ambient

170 PM extracts (Fe^{2+} and Cu^{2+}, Section 2.8) or the estimated abundance in ambient PM (CHP, HA, FA, and

171 H_2O_2, SI). To explore the influence of HA/FA on Fenton-like reactions, the radical formation in the

172 following aqueous mixtures was also analyzed: CHP+Fe^{2+}, CHP+Cu^{2+}, CHP+Cu^{2+}+HA, CHP+Cu^{2+}+FA.

173 The concentrations of Fe^{2+}, Cu^{2+}, HA, FA, and H_2O_2 in these solutions are 15-300 µM, 15-300 µM, 0-180

174 µg mL^{-1}, 0-180 µg mL^{-1}, 0-300 µM, respectively.

175 2.5 Quantification of radicals by EPR

176 5-tert-Butoxycarbonyl-5-methyl-1-pyrroline-N-oxide (BMPO) was used as a spin-trapping agent for

177 detecting different types of radicals formed in the extracts of PM. Ambient PM or laboratory-generated

178 SOA were extracted from Teflon filters into 10 mM BMPO neutral saline or water solutions by vortex

179 shaking for ~15 minutes (with Heidolph Reax 1). Around one fourth of each ambient PM filter or a whole

180 SOA-loaded filter was used for extraction. It was assumed that most of the short-lived radicals have reacted

181 with BMPO to form stable adducts during the extraction process.

182 A continuous-wave electron paramagnetic resonance (CW-EPR) X-band spectrometer (EMXplus-10/12;

183 Bruker Corporation) was applied for the identification and quantification of radical adducts (Tong et al.,

184 2016a;Tong et al., 2017;Tong et al., 2018;Tong et al., 2019). In order to increase the signal to noise ratio

185 of EPR spectra, some of the extracts were concentrated by a factor of 5 - 20 through 15 - 20 minutes drying

186 under 1-2 bar pure N_2 flow. The EPR spectra of BMPO-radical adducts were recorded by setting the

187 following operating parameters: a microwave frequency of 9.84 GHz, a microwave power of 0.017 mW

188 (20 dB), a receiver gain of 40 dB, a modulation amplitude of 1 G, a scan number of 50, a sweep width of

189 100 G, a modulation frequency of 100 kHz, a conversion time of 11 ms, and a time constant of 10 ms.

190 To average EPR spectra of different $PM_{2.5}$ extracts for each site, the magnetic field values of each

191 spectrum was transformed to g-values. Then we used the Bruker software, Xenon to do the averaging,

192 irrespective of the concentrations of $PM_{2.5}$ in extracts. The spin-counting method embedded in Xenon was

193 applied to quantify radical adducts. The spin-counting method was calibrated using the standard compound

194 4-hydroxy-2,2,6,6-tetramethylpiperidin-1-oxyl (TEMPOL). To obtain the relative yields of $^•OH$, $O_2^{•-}$, C-

195 and O-centered organic radicals, EPR spectra were simulated and fitted using the Xenon software before

196 deconvolution (Arangio et al., 2016;Tong et al., 2018). The spin number of assigned species accounts on

197 average for more than 95% of totally observed radical adducts, which is characterized by the peak area

198 ratios of corresponding species. EPR spectra with low signal-to-noise ratio introduce uncertainty into the

199 parameters describing the lineshape of peaks representing radical adducts (Tseitlin et al., 2012), causing a

200 total quantification uncertainty of 0-19% for different types of radicals ($^•OH$, $O_2^{•-}$, C- and O-centered

201 organic radicals etc.). The hyperfine coupling constants used for spectrum fitting are shown in Table S2.

202 More information on the hyperfine coupling constants of different types of BMPO radical adducts can be

203 found in previous studies (Zhao et al., 2001;Arangio et al., 2016).

2.6 Measurement of H_2O_2 yields

205 We extracted ambient $PM_{2.5}$ from one fourth of each Teflon filter into 1 mL ultra-pure water or neutral

206 saline by stirring it with a vortex shaker for ~15 minutes. Afterwards, the extracts were centrifuged at 9000

207 rpm (Eppendorf Minispin) for 3 minutes to remove the insoluble particles. Finally, the concentration of

208 H_2O_2 in the supernatant was measured using the MAK165 assay kit (Yan et al., 2017;Tong et al., 2018). 50

209 µL of supernatant and 50 µL of a Master Mix solution containing horseradish peroxidase and Amplex Red

210 substrate were mixed in a 96-well plate. The horseradish peroxidase catalyzed the oxidation of Amplex Red

211 by H_2O_2 to form fluorescent resorufin (Wang et al., 2017), which was consequently quantified using a

212 microplate reader (Synergy™ NEO, BioTek, excitation at 540 nm and emission at 590 nm) after 30 minutes

213 of incubation. The concentration of H_2O_2 in aqueous PM extracts was determined using an H_2O_2 calibration

214 curve based on standard H_2O_2 solutions and also corrected by blank measurements (Tong et al., 2018).

2.7 Mass spectrometry of organic compounds

216 By using a Q-Exactive Orbitrap mass spectrometer (Thermo Fisher Scientific, MA, USA) coupled with an

217 ultra-high performance liquid chromatography (UHPLC) system (Dionex UltiMate 3000, Thermo

218 Scientific, Germany) (Wang et al., 2018a;Wang et al., 2019;Tong et al., 2019), we characterized the HOM

219 and aromatic compounds in Hyytiälä, Mainz, and Beijing winter fine PM samples in negative ionization

220 mode. We processed the MS spectrum and UHPLC chromatogram of measured samples through a non-

221 target screening approach by using the commercially available software SIEVE® (Thermo Fisher Scientific,

222 MA, USA). Then, we blank-corrected the signals with peak intensity $> 1 \times 10^5$. Afterwards, we used the

223 following criteria to assign molecular formulae and filter out the irrational ones: (a) the number of atoms

224 of C, H, O, N, S, and Cl should be in the range of 1-39, 1-72, 0-20, 0-7, 0-4, and 0-2, respectively. (b)

225 Atomic ratios of H/C, O/C, N/C, S/C, and Cl/C should be in the range of 0.3-3, 0-3, 0-1.3, 0-0.8, and 0-0.8,

226 respectively.

227   The HOM is defined as formulae in the following chemical composition range of $C_xH_yO_z$: monomers

228   with x = 8–10, y = 12–16, z = 6–12, and z/x > 0.7; dimers with x = 17–20, y = 26–32 and z = 8–18 (Ehn et

229   al., 2014;Tröstl et al., 2016;Tong et al., 2019). Aromatics in this study are defined to be compounds with

230   aromaticity index (AI) > 0.5 and aromaticity equivalent (X_c) > 2.5, with the parameters accounting for the

231   fraction of oxygen and sulfur atoms involved in π-bond structures of a compound to be set as 1 (Koch and

232   Dittmar, 2006;Yassine et al., 2014;Tong et al., 2016b). Beyond this, the relative abundance of HOM or

233   aromatic compounds is defined to be the sum chromatographic area of HOM or aromatics divided by the

234   sum chromatographic area of all assigned organic compounds, with < 30% of totally detected organic

235   compounds not assigned (Wang et al., 2018a).

236   **2.8 Determination of water-soluble transition metal concentrations**

237   Based on the same extraction method as the H_2O_2 analysis in section 2.6, the concentrations of five selected

238   water-soluble transition metal species (Fe, Cu, Mn, Ni and V) in the supernatants of $PM_{2.5}$ extracts were

239   quantified using an inductively coupled plasma mass spectrometer (ICP-MS, Agilent 7900). These five

240   transition metal species were chosen for analysis due to their prominent concentrations and higher oxidative

241   potential (Charrier and Anastasio, 2012). A calibration curve for the ICP-MS analysis was made by

242   measuring standard multi-element stock solutions (Custom Grade, Inorganic Ventures). An aliquot of the

243   supernatants was diluted and acidified using a mixture of nitric acid (5%) and hydrofluoric acid (1%), which

244   was finalized to be 5 mL before analysis. The measured transition metal concentrations were blank-

245   corrected and shown in corresponding figures. The detection limit of the ICP-MS analysis in this study was

246   typically < 40 ng L^{-1}. The $PM_{2.5}$ samples collected on 2 June, 7 June, 9 June, 12 June in 2017 in Hyytiälä,

247   on 22 August, 26 August, 28 August, 25 September, 25 October, 14 November in 2017 in Mainz, and all

248   the 12 $PM_{2.5}$ samples from Beijing winter were used for transition metal analysis. Temporal evolution of

249   water-soluble transition metal concentrations in water extracts of Mainz $PM_{2.5}$ were also measured, and we

250   found that the total ion concentration of Fe, Cu, Mn, Ni, and V showed a rapid rise during the first 15 min

251   (Figure S2a), but at a much slower rate afterwards (Figure S2b).

3 Results and discussion

3.1 Aqueous-phase radical formation from ambient PM$_{2.5}$

Figure 2a shows averaged EPR spectra of BMPO-radical adducts in neutral saline extracts of PM$_{2.5}$ samples from Hyytiälä, Mainz, and Beijing (Table S1). Each spectrum is composed of multiple peaks attributable to different types of BMPO-radical adducts. The dotted vertical lines with different colors indicate the peaks attributable to adducts of BMPO with $^{\bullet}$OH (green), O$_2^{\bullet-}$ (orange), C- (blue) and O-centered organic radicals (purple) (Zhao et al., 2001;Arangio et al., 2016), respectively. The spectrum of Hyytiälä PM$_{2.5}$ is dominated by peaks attributable to C-centered radicals, the spectrum of Mainz PM$_{2.5}$ exhibits strong peaks attributable to C-centered radicals and $^{\bullet}$OH, and the spectrum of Beijing winter PM$_{2.5}$ is dominated by four peaks attributable to $^{\bullet}$OH.

Figure 2b shows the relative fractions (RF$_{spin}$) of $^{\bullet}$OH, O$_2^{\bullet-}$, C- and O-centered organic radicals averaged over multiple samples from each site. The mean RF of C- and O-centered organic radicals, respectively, were found to decrease from clean forest air samples (Hyytiälä, 66% and 11%) to polluted urban air samples (Mainz, 46% and 10%; Beijing, 39% and 5%). The high yield of C-centered radicals can be explained by rapid trapping of C-centered organic radicals (R$^{\bullet}$) by BMPO in the liquid phase (De Araujo et al., 2006). In the aqueous extracts, we applied a large excess of BMPO (10 mM of BMPO vs. ~1 µM of trapped radicals), and the estimated pseudo-first-order rate coefficient for R$^{\bullet}$ reacting with BMPO (9×10^5 s^{-1}, (Tong et al., 2018)) is much higher than the estimated R$^{\bullet}$ recombination rate coefficient (2.4×10^3, (Simic et al., 1969;Tong et al., 2018)). Moreover, rearrangement reactions in water can convert RO$^{\bullet}$ into R$^{\bullet}$ (Chevallier et al., 2004), which may warrant further investigation. The detected organic radicals are likely to comprise different molecular sizes and structures, as supported by our recent observations of organic radicals with up to 20 carbon atoms (C1-C20) formed by laboratory-generated SOA in water (Tong et al., 2018). The mean RF of $^{\bullet}$OH was found to increase from clean forest air samples (Hyytiälä, 21%) to polluted urban air samples (Mainz 38%, Beijing 53%). The mean RF of O$_2^{\bullet-}$ varied in the range of 2-6%, showing no clear trend beyond the standard errors indicated in Figure 2b.

277   The formation of organic radicals, $^\bullet OH$, $O_2^{\bullet -}$, and H_2O_2 can be attributed to Fenton-like reactions and

278   redox chemistry of organic and inorganic particulate matter, including environmentally persistent free

279   radicals (EPFR), highly oxygenated organic molecules (HOM), humic-like substances (HULIS), and

280   transition metal ions (Chevallier et al., 2004;Valavanidis et al., 2005;Li et al., 2008;Page et al.,

281   2012;Gehling et al., 2014;Tong et al., 2016a;Tong et al., 2017;Tong et al., 2018;Tong et al., 2019;Qiu et

282   al., 2020;Arangio et al., 2016). We speculate that hydrolytic or thermal decomposition of ROOH may play

283   a major role in the formation of RS by $PM_{2.5}$ from remote forest locations like Hyytiälä, where large

284   fractions of peroxide-containing HOM have been detected (Mutzel et al., 2015;Tröstl et al., 2016;Tong et

285   al., 2019;Pye et al., 2019;Roldin et al., 2019;Bianchi et al., 2019). ROOH can generate $^\bullet OH$ and O-centered

286   organic radicals through decomposition (ROOH $\rightarrow RO^\bullet + {}^\bullet OH$) and Fenton-like reactions (Fe^{2+} + ROOH

287    $\rightarrow Fe^{3+} + RO^\bullet + OH^-$; Fe^{2+} + ROOH$\rightarrow Fe^{3+} + RO^- + OH^\bullet$) (Tong et al., 2016a). Interconversion of $RO^\bullet$, $R^\bullet$

288   and $ROO^\bullet$ radicals can lead to the formation of $O_2^{\bullet -}$ and H_2O_2 (Chevallier et al., 2004;Tong et al., 2018),

289   which can further react with Fe^{2+} to form $^\bullet OH$ ($Fe^{2+} + H_2O_2 \rightarrow Fe^{3+} + {}^\bullet OH + OH^-$). In $PM_{2.5}$ from urban areas,

290   transition metal ions and HULIS are expected to play a major role in aqueous-phase formation and

291   interconversion of $^\bullet OH$, $O_2^{\bullet -}$ and H_2O_2 (Lloyd et al., 1997;Valavanidis et al., 2000;Zheng et al.,

292   2013;Hayyan et al., 2016;Lakey et al., 2016;Tan et al., 2016;Kuang et al., 2017;Ma et al., 2018;Li et al.,

293   2019).

294   Environmentally persistent free radicals (EPFR), are known to pre-exist in $PM_{2.5}$ at mass-specific

295   concentration levels of ~0.2 to ~2 pmol μg^{-1}, which are an order of magnitude higher than the typical mass-

296   specific aqueous-phase radical yields of ~0.02 to ~0.2 pmol μg^{-1} (Arangio et al., 2016;Vejerano et al.,

297   2018;Tong et al., 2019;Chen et al., 2020). While some EPFR may be water-insoluble (Chen et al., 2018),

298   others may directly contribute to the C-centered and O-centered radicals trapped by BMPO or participate

299   in redox reactions yielding $^\bullet OH$ and $O_2^{\bullet -}$ radicals (Khachatryan et al., 2011;Arangio et al., 2016). The latter

300   have such short chemical lifetimes that they have to be formed upon dissolution of the investigated samples

301   immediately prior to trapping by BMPO.

302   The experiments and data presented in this study provide exploratory perspectives of the pathways of

303   formation and interconversion of reactive species formed by $PM_{2.5}$ in the aqueous-phase, including highly

304   reactive radicals and less reactive reservoir species like H_2O_2 as discussed below. A quantitative assessment,

305   mechanistic elucidation, and full understanding will require comprehensive further experimental

306   investigations and model calculations.

307   **3.2 Yields of aqueous-phase radicals and H_2O_2 from ambient $PM_{2.5}$**

308   Figure 3 shows the average air volume-specific yields and $PM_{2.5}$ mass-specific yields of aqueous-phase

309   reactive species (RS), including radicals and H_2O_2, plotted against the $PM_{2.5}$ mass concentrations observed

310   during the sampling periods in Hyytiälä, Mainz, and Beijing, respectively. The volume-specific yields refer

311   to the sampled air volume and are given in units of pmol m^{-3}. They represent the absolute amounts of RS

312   that are formed when the particulate matter is deposited in an aqueous phase such as cloud water or

313   epithelial lining fluid, where they can contribute to atmospheric multiphase chemistry, oxidative stress and

314   adverse health effect of PM respectively (Lakey et al., 2016;Tong et al., 2018). The mass-specific yields

315   are normalized by the sampled mass of $PM_{2.5}$ and given in units of pmol µg^{-1}. They represent the relative

316   amounts of aqueous RS formed per mass unit $PM_{2.5}$, enabling a direct comparison of the relative reactivity

317   and aqueous RS-forming potential of the fine particulate matter from different sampling sites.

318   As illustrated in Figure 3a, the $PM_{2.5}$ concentration increased by more than an order of magnitude

319   between the samples from Hyytiälä and Beijing (from ~5 to ~200 µg m^{-3}), and the volume-specific yield of

320   aqueous-phase H_2O_2 exhibited a similarly strong increase (from ~10 to ~200 µg m^{-3}), while the volume-

321   specific yield of aqueous-phase radicals exhibited a much smaller increase (from ~3 to ~7 pmol m^{-3}; Tables

322   S1, S4, and S5). The strong increase of H_2O_2 with increasing $PM_{2.5}$ concentration is consistent with earlier

323   studies identifying a wide range of redox-active organic and inorganic aerosol components that can produce

324   H_2O_2 in the aqueous phase (Gunz and Hoffmann, 1990;Anastasio et al., 1994;Zuo and Deng,

325   1997;Arellanes et al., 2006;Chung et al., 2006;Hua et al., 2008;Möller, 2009;Wang et al., 2010;Wang et al.,

326   2012;Anglada et al., 2015;Herrmann et al., 2015;Lakey et al., 2016;Tong et al., 2018;Bianco et al., 2020).

327   As illustrated in Figure 3b, the average mass-specific yields of aqueous-phase H_2O_2 were similar for the

328   investigated urban and forest $PM_{2.5}$ samples (around 2-4 pmol μg^{-1}). In contrast, the mass-specific yield of

329   aqueous-phase radicals was highest for the forest samples (~0.6 pmol μg^{-1}) and decreased steeply with

330   increasing $PM_{2.5}$ mass concentration for the urban samples (~0.3 pmol μg^{-1} for Mainz, ~0.06 pmol μg^{-1} for

331   Beijing). Accordingly, the relative fraction of radicals compared to H_2O_2 formed and detected in the

332   aqueous phase decreased from 22% for the $PM_{2.5}$ samples from Hyytiälä to 8% for Mainz and 3% for

333   Beijing. In other words, the aqueous H_2O_2-forming potential per mass unit of $PM_{2.5}$ was roughly the same

334   for all investigated samples, whereas the aqueous radical-forming potential varied widely between the

335   different samples.

336   The observed negative correlation with $PM_{2.5}$ mass concentration suggests that the mass-specific yield

337   of aqueous-phase radicals from fine particulate matter may be influenced by the sample load and level of

338   concentration in aqueous extracts, e.g., through enhanced re-combination of radicals at elevated

339   concentration. Experiments performed at different dilutions, i.e., with varying aqueous extract volumes and

340   concentration levels, however, suggest that observed differences in radical forming potential were not just

341   due to different sample loads but influence by differences in the chemical composition and reactivity of the

342   investigated $PM_{2.5}$ samples (Figure S1d and S1e). For example, the particularly high mass-specific yields

343   of total radicals and C-centered radicals in the aqueous phase appears associated with particularly high mass

344   fractions of organic matter in $PM_{2.5}$ from Hyytiälä (~70%, (Jimenez et al., 2009;Maenhaut et al., 2011)).

345   Figure 4 shows how the relative fractions (RF_{spin}) of C-centered radicals and $^{\bullet}OH$ in the aqueous phase

346   varied with the abundance of HOM, aromatic compounds, and water-soluble transition metal ions in the

347   investigated $PM_{2.5}$ samples (Hyytiälä and Mainz) or $PM_{2.5}$ collected at different times (Beijing). As

348   illustrated in Figure 4a, C-centered radicals exhibited a pronounced increase with increasing HOM; whereas

349    $^{\bullet}OH$ radicals showed a near-linear decrease. The observed increase of C-centered radicals with HOM is

350   consistent with earlier studies indicating that peroxide-containing HOM may play an important role in

351   organic radical formation (Tong et al., 2016a;Tong et al., 2019). In contrast, the C-centered radicals did not

352 exhibit an increase but a decrease with increasing abundance of aromatic compounds (Figure 4b). This is

353 consistent with ability of certain aromatic compounds like quinones and semiquinones to enhance redox

354 cycling and the formation of $^\bullet$OH radicals in analogy to Fenton reactions (Chung et al., 2006;Zhang and

355 Tao, 2009;Khachatryan et al., 2011;Elser et al., 2016;Fan et al., 2016;Lakey et al., 2016;An et al., 2019).

356 As illustrated in Figure 4c, C-centered radicals exhibited a pronounced decrease with transition metal ions,

357 whereas $^\bullet$OH radicals exhibited a near-linear increase. These findings are consistent with the role of

358 transition metal ions in Fenton-like reactions efficiently converting H_2O_2 and hydroperoxides into $^\bullet$OH

359 radicals, and with studies reporting that metal-organic interactions may alter the oxidative potential

360 particulate matter under atmospheric and physiological conditions (Zuo and Hoigne, 1992;Lakey et al.,

361 2016;Singh and Gupta, 2016;Cheng et al., 2017;Wang et al., 2018b;Wei et al., 2019;Lin and Yu, 2020). To

362 gain further insights into the complex interactions of organic particulate matter, transition metal ions, and

363 reactive species in the aqueous phase, we performed experiments with laboratory-generated secondary

364 organic aerosols and surrogate mixtures of atmospherically relevant substance classes as detailed in the

365 following sections.

366 **3.3 Aqueous-phase radical yields of laboratory-generated SOA**

367 To investigate the influence of biogenic and anthropogenic secondary organic aerosols (SOA) on aqueous-

368 phase radical formation, we performed experiments with SOA from naphthalene and β-pinene oxidized by

369 O_3 and $^\bullet$OH in a PAM chamber (Sect. 2.3).

370 As illustrated in Figure 5a, we found a steep non-linear increase of the mass-specific radical yield with

371 increasing precursor mass fraction of β-pinene from ~2 pmol µg^{-1} for pure naphthalene SOA to ~8 pmol

372 µg^{-1} for pure β-pinene SOA, which is consistent with related earlier investigations that found higher radical

373 yields for biogenic SOA compared to anthropogenic SOA (Tong et al., 2016a;Tong et al., 2017;Tong et al.,

374 2018;Tong et al., 2019).

375 Figure 5b shows that β-pinene SOA mainly generates $^\bullet$OH (~86%), whereas naphthalene SOA and

376 mixtures of naphthalene and β-pinene SOA mainly generate $O_2^{\bullet-}$ (60-77%) and C-centered radicals (18-

377   34%). Substantial formation of $O_2^{\bullet-}$ by terpene SOA is consistent with a recent study, showing that $O_2^{\bullet-}$

378   formation via $^\bullet$OH oxidation of primary or secondary alcohols followed by unimolecular decomposition of

379   α-hydroxyperoxyl radicals (Wei et al., 2021). The small RF of $^\bullet$OH generated by naphthalene SOA may

380   appear in contrast to the high RF of $^\bullet$OH generated $PM_{2.5}$ from Beijing that contains substantial amounts of

381   aromatics (Figure 4b). Note, however, that the composition of $PM_{2.5}$ from Beijing is much more complex

382   than that of laboratory-generated naphthalene SOA. For example, Fenton-like reactions of transition metal

383   ions are expected to generate $^\bullet$OH in ambient $PM_{2.5}$ (Kehrer, 2000;Tong et al., 2016a), whereas the

384   laboratory-generated SOA does not contain significant amounts of transition metals.

385   **3.4 Aqueous-phase radical yields of surrogate mixtures**

386   To investigate the influence of different types of redox-active components in $PM_{2.5}$ on the total yield of

387   radicals in the aqueous phase and on the relative fractions (RF_{spin}) of different types of radicals, we

388   performed experiments with aqueous surrogate mixtures of Fe^{2+}, Cu^{2+}, humic acid (HA), fulvic acid (FA),

389   cumene hydroperoxide (CHP), and H_2O_2 in varying concentrations. Figure 6 shows that increasing

390   concentrations of organic hydroperoxide (here CHP) can lead to a near-linear increase of total radical

391   concentration in the aqueous phase (Figure 6a), and to a strong increase of RF_{spin} for C-centered radicals

392   (Figure 6b). The increase of $R^\bullet$ with CHP is consistent with the high RF_{spin} for C-centered radicals in $PM_{2.5}$

393   from Hyytiälä (Figure 2b), which contains a large fraction of HOM (Tong et al., 2019). Increasing

394   concentrations of H_2O_2 also led to a near-linear increase of increase of total radical concentration in the

395   aqueous phase (Figure 6c) as well as a strong increase of $^\bullet$OH (Figure 6d). The strong increase of aqueous-

396   phase $^\bullet$OH with H_2O_2 indicates that gas-particle partitioning and multiphase chemical reactions of gas-

397   phase oxidants can substantially influence the generation of radicals and oxidative stress by ambient $PM_{2.5}$.

398   For increasing concentrations of humic acid (HA), we observed a strong non-linear decrease of total

399   radical concentration in the aqueous phase (Figure 6e), and to a strong increase of RF_{spin} for C-centered

400   radicals (Figure 6f). The decreasing radical concentration is likely due to the ability of HA to bind/chelate

401   iron and other metal ions (Graber and Rudich, 2006;Laglera and van den Berg, 2009;Scheinhardt et al.,

402 2013;Tang et al., 2014;Yang et al., 2017), which may lead to a suppression of radical formation via Fenton-

403 like reactions. Moreover, humic substances can act as antioxidants and radical scavengers (Aeschbacher et

404 al., 2012). The fractional increase of C-centered radicals reflects the involvement of HA in complex radical

405 chemistry (Shi et al., 2020). Compared to HA, the effects of fulvic acid (FA) were qualitatively similar but

406 quantitatively less pronounced (Figures. 6g and 6h), which is consistent with earlier studies investigating

407 the metal ion binding capacity and redox chemistry of FA (Wang et al., 1996;Graber and Rudich,

408 2006;Scheinhardt et al., 2013;Tang et al., 2014;Gonzalez et al., 2017;Yang et al., 2017). Different

409 reactivities of HA and FA are also reflected by the different RF values of $O_2^{\bullet-}$ and C-centered radicals

410 observed at high concentrations of FA and HA (Figure 6h vs. Figure 6f) as well as in reactions mixtures

411 with copper instead of iron ions (Figure S6). Further investigations will be required to resolve the

412 underlying reaction mechanisms and kinetics.

413 **4 Conclusions and implications**

414 In this study, we investigated the formation of aqueous-phase H_2O_2 and radicals by aerosol samples from

415 remote forest and polluted urban air. The aqueous H_2O_2-forming potential per mass unit of $PM_{2.5}$ was

416 roughly the same for all investigated samples, whereas the mass-specific yields of radicals were lower for

417 sampling sites with higher concentration of ambient $PM_{2.5}$.

418 The abundances of water-soluble transition metals in ambient $PM_{2.5}$ were positively correlated with the

419 relative fraction of $^{\bullet}OH$ and negatively correlated with the relative fraction of carbon-centered radicals,

420 which can be attributed to Fenton-like reactions. In contrast, HOM was negatively correlated with the

421 relative fraction of $^{\bullet}OH$ and positively correlated with the relative fraction of carbon-centered radicals,

422 which is consistent with related earlier studies indicating that peroxide-containing HOM may play an

423 important role in organic radical formation (Tong et al., 2016a;Tong et al., 2019).

424 We found that the relative fractions of different types of radicals formed by ambient $PM_{2.5}$ were

425 comparable to surrogate mixtures comprising transition metal ions, organic hydroperoxide, H_2O_2, and

426 humic or fulvic acids. Our results show that the interplay of transition metal ions (e.g., iron and copper

427 ions), highly oxidized organic molecules (e.g., hydroperoxides), and complexing or scavenging agents (e.g.,

428 humic or fulvic acids) leads to non-linear concentration dependencies in the aqueous-phase RS production.

429 A strong dependence on chemical composition was also observed for the aqueous-phase radical yields of

430 laboratory-generated SOA from precursor mixtures of naphthalene and β-pinene.

431   Overall, our findings show how the composition of $PM_{2.5}$ can influence the amount and nature of

432 aqueous-phase RS, which may explain differences in the chemical reactivity and health effects of particulate

433 matter in clean and polluted air. Further investigations will be required to resolve the influence of biogenic

434 and anthropogenic pollutants on atmospheric chemistry, air quality, and public health in the Anthropocene

435 (Pöschl and Shiraiwa, 2015;Cheng et al., 2016;Shiraiwa et al., 2017;An et al., 2019;Roldin et al.,

436 2019;Daellenbach et al., 2020;Fang et al., 2020;Lelieveld et al., 2020;Lin and Yu, 2020;Pöschl, 2020;Su et

437 al., 2020;Tao et al., 2020;Yun et al., 2020;Zheng et al., 2020;Wang et al., 2021).

References

438 **References**

439 Aeschbacher, M., Graf, C., Schwarzenbach, R. P., and Sander, M.: Antioxidant properties of humic

440 substances, Environ. Sci. Technol., 46, 4916-4925, 2012.

441 An, Z., Huang, R.-J., Zhang, R., Tie, X., Li, G., Cao, J., Zhou, W., Shi, Z., Han, Y., and Gu, Z.: Severe

442 haze in Northern China: A synergy of anthropogenic emissions and atmospheric processes, Proc. Natl. Acad.

443 Sci. U.S.A., 116, 8657-8666, 2019.

444 Anastasio, C., Faust, B. C., and Allen, J. M.: Aqueous phase photochemical formation of hydrogen peroxide

445 in authentic cloud waters, J. Geophys. Res. Atmos., 99, 8231-8248, 1994.

446 Anglada, J. M., Martins-Costa, M., Francisco, J. S., and Ruiz-Lopez, M. F.: Interconnection of reactive

447 oxygen species chemistry across the interfaces of atmospheric, environmental, and biological processes,

448 Acc. Chem. Res., 48, 575-583, 2015.

449 Arangio, A. M., Tong, H., Socorro, J., Pöschl, U., and Shiraiwa, M.: Quantification of environmentally

450 persistent free radicals and reactive oxygen species in atmospheric aerosol particles, Atmos. Chem. Phys.,

451 16, 13105-13119, 2016.

452 Arellanes, C., Paulson, S. E., Fine, P. M., and Sioutas, C.: Exceeding of Henry's law by hydrogen peroxide

453 associated with urban aerosols, Environ. Sci. Technol., 40, 4859-4866, 2006.

454 Badali, K., Zhou, S., Aljawhary, D., Antiñolo, M., Chen, W., Lok, A., Mungall, E., Wong, J., Zhao, R., and

455 Abbatt, J.: Formation of hydroxyl radicals from photolysis of secondary organic aerosol material, Atmos.

456 Chem. Phys., 15, 7831-7840, 2015.

457 Bates, J. T., Weber, R. J., Abrams, J., Verma, V., Fang, T., Klein, M., Strickland, M. J., Sarnat, S. E., Chang,

458 H. H., and Mulholland, J. A.: Reactive oxygen species generation linked to sources of atmospheric

459 particulate matter and cardiorespiratory effects, Environ. Sci. Technol., 49, 13605-13612, 2015.

460 Bates, J. T., Fang, T., Verma, V., Zeng, L., Weber, R. J., Tolbert, P. E., Abrams, J. Y., Sarnat, S. E., Klein,

461 M., Mulholland, J. A., and Russell, A. G.: Review of acellular assays of ambient particulate matter oxidative

462 potential: Methods and relationships with composition, sources, and health effects, Environ. Sci. Technol.,

463 53, 4003-4019, 2019.

464 Baumgartner, J., Zhang, Y., Schauer, J. J., Huang, W., Wang, Y., and Ezzati, M.: Highway proximity and

465 black carbon from cookstoves as a risk factor for higher blood pressure in rural China, Proc. Natl. Acad.

466 Sci. U.S.A., 111, 13229-13234, 2014.

467 Bianchi, F., Kurtén, T., Riva, M., Mohr, C., Rissanen, M. P., Roldin, P., Berndt, T., Crounse, J. D.,

468 Wennberg, P. O., and Mentel, T. F.: Highly oxygenated organic molecules (HOM) from gas-phase

469 autoxidation involving peroxy radicals: A key contributor to atmospheric aerosol, Chem. Rev., 119, 3472-

470 3509, 2019.

Bianco, A., Passananti, M., Brigante, M., and Mailhot, G.: Photochemistry of the Cloud Aqueous Phase: A Review, Molecules, 25, 423, 2020.

Catrouillet, C., Davranche, M., Dia, A., Bouhnik-Le Coz, M., Marsac, R., Pourret, O., and Gruau, G.: Geochemical modeling of Fe (II) binding to humic and fulvic acids, Chem. Geol., 372, 109-118, 2014.

Charrier, J., and Anastasio, C.: On dithiothreitol (DTT) as a measure of oxidative potential for ambient particles: evidence for the importance of soluble transition metals, Atmos. Chem. Phys., 12, 9321-9333, 2012.

Charrier, J. G., McFall, A. S., Richards-Henderson, N. K., and Anastasio, C.: Hydrogen peroxide formation in a surrogate lung fluid by transition metals and quinones present in particulate matter, Environ. Sci. Technol., 48, 7010-7017, 2014.

Charrier, J. G., and Anastasio, C.: Rates of hydroxyl radical production from transition metals and quinones in a surrogate lung fluid, Environ. Sci. Technol., 49, 9317-9325, 2015.

Chen, Q., Sun, H., Wang, M., Mu, Z., Wang, Y., Li, Y., Wang, Y., Zhang, L., and Zhang, Z.: Dominant fraction of EPFRs from nonsolvent-extractable organic matter in fine particulates over Xi'an, China, Environ. Sci. Technol., 52, 9646-9655, 2018.

Chen, Q., Sun, H., Song, W., Cao, F., Tian, C., and Zhang, Y.-L.: Size-resolved exposure risk of persistent free radicals (PFRs) in atmospheric aerosols and their potential sources, Atmos. Chem. Phys., 20, 14407-14417, 2020.

Chen, X., Hopke, P. K., and Carter, W. P.: Secondary organic aerosol from ozonolysis of biogenic volatile organic compounds: chamber studies of particle and reactive oxygen species formation, Environ. Sci. Technol., 45, 276-282, 2010.

Cheng, C., Li, M., Chan, C. K., Tong, H., Chen, C., Chen, D., Wu, D., Li, L., Wu, C., and Cheng, P.: Mixing state of oxalic acid containing particles in the rural area of Pearl River Delta, China: implications for the formation mechanism of oxalic acid, Atmos. Chem. Phys., 17, 9519-9533, 2017.

Cheng, Y., Zheng, G., Wei, C., Mu, Q., Zheng, B., Wang, Z., Gao, M., Zhang, Q., He, K., and Carmichael, G.: Reactive nitrogen chemistry in aerosol water as a source of sulfate during haze events in China, Sci. Adv., 2, e1601530, 2016.

Chevallier, E., Jolibois, R. D., Meunier, N., Carlier, P., and Monod, A.: "Fenton-like" reactions of methylhydroperoxide and ethylhydroperoxide with Fe^{2+} in liquid aerosols under tropospheric conditions, Atmos. Environ., 38, 921-933, 2004.

Chowdhury, P. H., He, Q., Carmieli, R., Li, C., Rudich, Y., and Pardo, M.: Connecting the Oxidative Potential of Secondary Organic Aerosols with Reactive Oxygen Species in Exposed Lung Cells, Environ. Sci. Technol., 53, 13949-13958, 2019.

Chung, M. Y., Lazaro, R. A., Lim, D., Jackson, J., Lyon, J., Rendulic, D., and Hasson, A. S.: Aerosol-borne quinones and reactive oxygen species generation by particulate matter extracts, Environ. Sci. Technol., 40, 4880-4886, 2006.

Crobeddu, B., Baudrimont, I., Deweirdt, J., Sciare, J., Badel, A., Camproux, A.-C., Bui, L. C., and Baeza-Squiban, A.: Lung Antioxidant Depletion: A Predictive Indicator of Cellular Stress Induced by Ambient Fine Particles, Environ. Sci. Technol., 54, 2360-2369, 2020.

Cui, Y., Xie, X., Jia, F., He, J., Li, Z., Fu, M., Hao, H., Liu, Y., Liu, J. Z., and Cowan, P. J.: Ambient fine particulate matter induces apoptosis of endothelial progenitor cells through reactive oxygen species formation, Cell Physiol. Biochem., 35, 353-363, 2015.

Daellenbach, K. R., Uzu, G., Jiang, J., Cassagnes, L.-E., Leni, Z., Vlachou, A., Stefenelli, G., Canonaco, F., Weber, S., and Segers, A.: Sources of particulate-matter air pollution and its oxidative potential in Europe, Nature, 587, 414-419, 2020.

De Araujo, M., De M. Carneiro, J., and Taranto, A.: Solvent effects on the relative stability of radicals derived from artemisinin: DFT study using the PCM/COSMO approach, Int. J. Quantum. Chem., 106, 2804-2810, 2006.

Donaldson, D., and Valsaraj, K. T.: Adsorption and reaction of trace gas-phase organic compounds on atmospheric water film surfaces: A critical review, Environ. Sci. Technol., 44, 865-873, 2010.

Ehn, M., Thornton, J. A., Kleist, E., Sipilä, M., Junninen, H., Pullinen, I., Springer, M., Rubach, F., Tillmann, R., and Lee, B.: A large source of low-volatility secondary organic aerosol, Nature, 506, 476-479, 2014.

Elser, M., Huang, R.-J., Wolf, R., Slowik, J. G., Wang, Q., Canonaco, F., Li, G., Bozzetti, C., Daellenbach, K. R., and Huang, Y.: New insights into $PM_{2.5}$ chemical composition and sources in two major cities in China during extreme haze events using aerosol mass spectrometry, Atmos. Chem. Phys., 16, 3207-3225, 2016.

Enami, S., Sakamoto, Y., and Colussi, A. J.: Fenton chemistry at aqueous interfaces, Proc. Natl. Acad. Sci. U.S.A., 111, 623-628, 2014.

Ervens, B., Turpin, B., and Weber, R.: Secondary organic aerosol formation in cloud droplets and aqueous particles (aqSOA): a review of laboratory, field and model studies, Atmos. Chem. Phys., 11, 11069-11102, 2011.

Fan, X., Wei, S., Zhu, M., Song, J., and Peng, P. a.: Comprehensive characterization of humic-like substances in smoke $PM_{2.5}$ emitted from the combustion of biomass materials and fossil fuels, Atmos. Chem. Phys., 16, 13321-13340, 2016.

536 Fang, T., Guo, H., Verma, V., Peltier, R., and Weber, R.: $PM_{2.5}$ water-soluble elements in the southeastern
537 United States: automated analytical method development, spatiotemporal distributions, source
538 apportionment, and implications for heath studies, Atmos. Chem. Phys., 15, 11667-11682, 2015.

539 Fang, T., Verma, V., Bates, J. T., Abrams, J., Klein, M., Strickland, M. J., Sarnat, S. E., Chang, H. H.,
540 Mulholland, J. A., and Tolbert, P. E.: Oxidative potential of ambient water-soluble $PM_{2.5}$ in the southeastern
541 United States: contrasts in sources and health associations between ascorbic acid (AA) and dithiothreitol
542 (DTT) assays, Atmos. Chem. Phys., 16, 3865-3879, 2016.

543 Fang, T., Lakey, P. S. J., Weber, R. J., and Shiraiwa, M.: Oxidative Potential of Particulate Matter and
544 Generation of Reactive Oxygen Species in Epithelial Lining Fluid, Environ. Sci. Technol., 53, 12784-12792,
545 2019.

546 Fang, T., Lakey, P. S. J., Rivera-Rios, J. C., Keutsch, F. N., and Shiraiwa, M.: Aqueous-Phase
547 Decomposition of Isoprene Hydroxy Hydroperoxide and Hydroxyl Radical Formation by Fenton-Like
548 Reactions with Iron Ions, J. Phys. Chem. A, 124, 5230-5236, 2020.

549 Gehling, W., Khachatryan, L., and Dellinger, B.: Hydroxyl radical generation from environmentally
550 persistent free radicals (EPFRs) in $PM_{2.5}$, Environ. Sci. Technol., 48, 4266-4272, 2014.

551 Gilardoni, S., Massoli, P., Paglione, M., Giulianelli, L., Carbone, C., Rinaldi, M., Decesari, S., Sandrini, S.,
552 Costabile, F., and Gobbi, G. P.: Direct observation of aqueous secondary organic aerosol from biomass-
553 burning emissions, Proc. Natl. Acad. Sci. U.S.A., 113, 10013-10018, 2016.

554 Gligorovski, S., Strekowski, R., Barbati, S., and Vione, D.: Environmental implications of hydroxyl radicals
555 ($^{\bullet}$OH), Chem. Rev., 115, 13051-13092, 2015.

556 Goldstein, A. H., Koven, C. D., Heald, C. L., and Fung, I. Y.: Biogenic carbon and anthropogenic pollutants
557 combine to form a cooling haze over the southeastern United States, Proc. Natl. Acad. Sci. U.S.A., 106,
558 8835-8840, 2009.

559 Gonzalez, D. H., Cala, C. K., Peng, Q., and Paulson, S. E.: HULIS enhancement of hydroxyl radical
560 formation from Fe(II): Kinetics of fulvic acid–Fe(II) complexes in the presence of lung antioxidants,
561 Environ. Sci. Technol., 51, 7676-7685, 2017.

562 Graber, E., and Rudich, Y.: Atmospheric HULIS: How humic-like are they? A comprehensive and critical
563 review, Atmos. Chem. Phys., 6, 729-753, 2006.

564 Gunz, D. W., and Hoffmann, M. R.: Atmospheric chemistry of peroxides: a review, Atmos. Environ., 24,
565 1601-1633, 1990.

566 Hakola, H., Hellén, H., Hemmilä, M., Rinne, J., and Kulmala, M.: In situ measurements of volatile organic
567 compounds in a boreal forest, Atmos. Chem. Phys., 12, 11665-11678, 2012.

568 Halliwell, B., and Whiteman, M.: Measuring reactive species and oxidative damage in vivo and in cell
569 culture: how should you do it and what do the results mean?, Br. J. Pharmacol., 142, 231-255, 2004.

Hari, P., and Kulmala, M.: Station for Measuring EcosystemsAtmosphere Relations (SMEAR II), Boreal Env. Res., 10, 315-322, 2005.

Hayyan, M., Hashim, M. A., and AlNashef, I. M.: Superoxide ion: generation and chemical implications, Chem. Rev., 116, 3029-3085, 2016.

Herrmann, H., Schaefer, T., Tilgner, A., Styler, S. A., Weller, C., Teich, M., and Otto, T.: Tropospheric aqueous-phase chemistry: kinetics, mechanisms, and its coupling to a changing gas phase, Chem. Rev., 115, 4259-4334, 2015.

Hoyle, C. R., Boy, M., Donahue, N. M., Fry, J. L., Glasius, M., Guenther, A., Hallar, A. G., Huff Hartz, K., Petters, M. D., and Petäjä, T.: A review of the anthropogenic influence on biogenic secondary organic aerosol, Atmos. Chem. Phys., 11, 321-343, 2011.

Hua, W., Chen, Z., Jie, C., Kondo, Y., Hofzumahaus, A., Takegawa, N., Chang, C., Lu, K., Miyazaki, Y., and Kita, K.: Atmospheric hydrogen peroxide and organic hydroperoxides during PRIDE-PRD'06, China: their concentration, formation mechanism and contribution to secondary aerosols, Atmos. Chem. Phys., 8, 6755-6773, 2008.

Huang, G., Liu, Y., Shao, M., Li, Y., Chen, Q., Zheng, Y., Wu, Z., Liu, Y., Wu, Y., Hu, M., Li, X., Lu, S., Wang, C., Liu, J., Zheng, M., and Zhu, T.: Potentially Important Contribution of Gas-Phase Oxidation of Naphthalene and Methylnaphthalene to Secondary Organic Aerosol during Haze Events in Beijing, Environ. Sci. Technol., 53, 1235-1244, 2019.

Huang, R.-J., Zhang, Y., Bozzetti, C., Ho, K.-F., Cao, J.-J., Han, Y., Daellenbach, K. R., Slowik, J. G., Platt, S. M., and Canonaco, F.: High secondary aerosol contribution to particulate pollution during haze events in China, Nature, 514, 218-222, 2014.

Jacob, D. J.: Heterogeneous chemistry and tropospheric ozone, Atmos. Environ., 34, 2131-2159, 2000.

Jimenez, J. L., Canagaratna, M., Donahue, N., Prevot, A., Zhang, Q., Kroll, J. H., DeCarlo, P. F., Allan, J. D., Coe, H., and Ng, N.: Evolution of organic aerosols in the atmosphere, Science, 326, 1525-1529, 2009.

Jin, L., Xie, J., Wong, C. K., Chan, S. K., Abbaszade, G. l., Schnelle-Kreis, J. r., Zimmermann, R., Li, J., Zhang, G., and Fu, P.: Contributions of city-specific fine particulate matter ($PM_{2.5}$) to differential in vitro oxidative stress and toxicity implications between Beijing and Guangzhou of China, Environ. Sci. Technol., 53, 2881-2891, 2019.

Kalyanaraman, B., Darley-Usmar, V., Davies, K. J., Dennery, P. A., Forman, H. J., Grisham, M. B., Mann, G. E., Moore, K., Roberts II, L. J., and Ischiropoulos, H.: Measuring reactive oxygen and nitrogen species with fluorescent probes: challenges and limitations, Free Radic. Biol. Med., 52, 1-6, 2012.

Kang, E., Root, M., Toohey, D., and Brune, W. H.: Introducing the concept of potential aerosol mass (PAM), Atmos. Chem. Phys., 7, 5727-5744, 2007.

Kehrer, J. P.: The Haber–Weiss reaction and mechanisms of toxicity, Toxicology, 149, 43-50, 2000.

Khachatryan, L., Vejerano, E., Lomnicki, S., and Dellinger, B.: Environmentally persistent free radicals (EPFRs). 1. Generation of reactive oxygen species in aqueous solutions, Environ. Sci. Technol., 45, 8559-8566, 2011.

Koch, B., and Dittmar, T.: From mass to structure: An aromaticity index for high‐resolution mass data of natural organic matter, Rapid Commun. Mass Spectrom., 20, 926-932, 2006.

Kostić, I., Anđelković, T., Nikolić, R., Bojić, A., Purenović, M., Blagojević, S., and Anđelković, D.: Copper(II) and lead(II) complexation by humic acid and humic-like ligands, J. Serb. Chem. Soc., 76, 1325-1336, 2011.

Kuang, X. M., Scott, J. A., da Rocha, G. O., Betha, R., Price, D. J., Russell, L. M., Cocker, D. R., and Paulson, S. E.: Hydroxyl radical formation and soluble trace metal content in particulate matter from renewable diesel and ultra low sulfur diesel in at-sea operations of a research vessel, Aerosol Sci. Technol., 51, 147-158, 2017.

Laakso, L., Hussein, T., Aarnio, P., Komppula, M., Hiltunen, V., Viisanen, Y., and Kulmala, M.: Diurnal and annual characteristics of particle mass and number concentrations in urban, rural and Arctic environments in Finland, Atmos. Environ., 37, 2629-2641, 2003.

Laglera, L. M., and van den Berg, C. M.: Evidence for geochemical control of iron by humic substances in seawater, Limnol. Oceanogr., 54, 610-619, 2009.

Lakey, P. S., Berkemeier, T., Tong, H., Arangio, A. M., Lucas, K., Pöschl, U., and Shiraiwa, M.: Chemical exposure-response relationship between air pollutants and reactive oxygen species in the human respiratory tract, Sci. Rep., 6, 32916, 2016.

Lammel, G., Kitanovski, Z., Kukucka, P., Novak, J., Arangio, A. M., Codling, G. P., Filippi, A., Hovorka, J., Kuta, J., and Leoni, C.: Oxygenated and Nitrated Polycyclic Aromatic Hydrocarbons in Ambient Air—Levels, Phase Partitioning, Mass Size Distributions, and Inhalation Bioaccessibility, Environ. Sci. Technol., 54, 2615-2625, 2020.

Landreman, A. P., Shafer, M. M., Hemming, J. C., Hannigan, M. P., and Schauer, J. J.: A macrophage-based method for the assessment of the reactive oxygen species (ROS) activity of atmospheric particulate matter (PM) and application to routine (daily-24 h) aerosol monitoring studies, Aerosol Sci. Technol., 42, 946-957, 2008.

Lelieveld, J., and Pöschl, U.: Chemists can help to solve the air-pollution health crisis, Nature, 551, 291-293, 2017.

Lelieveld, J., Pozzer, A., Pöschl, U., Fnais, M., Haines, A., and Münzel, T.: Loss of life expectancy from air pollution compared to other risk factors: a worldwide perspective, Cardiovasc. Res., doi:10.1093/cvr/cvaa025, 2020.

637   Li, N., Xia, T., and Nel, A. E.: The role of oxidative stress in ambient particulate matter-induced lung

638   diseases and its implications in the toxicity of engineered nanoparticles, Free Radic. Biol. Med., 44, 1689-

639   1699, 2008.

640   Li, X., Kuang, X. M., Yan, C., Ma, S., Paulson, S. E., Zhu, T., Zhang, Y., and Zheng, M.: Oxidative

641   potential by $PM_{2.5}$ in the North China Plain: generation of hydroxyl radical, Environ. Sci. Technol., 53,

642   512-520, 2018.

643   Li, X., Han, J., Hopke, P. K., Hu, J., Shu, Q., Chang, Q., and Ying, Q.: Quantifying primary and secondary

644   humic-like substances in urban aerosol based on emission source characterization and a source-oriented air

645   quality model, Atmos. Chem. Phys., 19, 2327-2341, 2019.

646   Lin, M., and Yu, J. Z.: Assessment of interactions between transition metals and atmospheric organics:

647   Ascorbic Acid Depletion and Hydroxyl Radical Formation in Organic-metal Mixtures, Environ. Sci.

648   Technol., 54, 1431−1442, 2020.

649   Lin, P., and Yu, J. Z.: Generation of reactive oxygen species mediated by humic-like substances in

650   atmospheric aerosols, Environ. Sci. Technol., 45, 10362-10368, 2011.

651   Lin, Y., Ma, Y., Qiu, X., Li, R., Fang, Y., Wang, J., Zhu, Y., and Hu, D.: Sources, transformation, and

652   health implications of PAHs and their nitrated, hydroxylated, and oxygenated derivatives in $PM_{2.5}$ in Beijing,

653   J. Geophys. Res. Atmos., 120, 7219-7228, 2015.

654   Liu, F., Saavedra, M. G., Champion, J. A., Griendling, K. K., and Ng, N. L.: Prominent Contribution of

655   Hydrogen Peroxide to Intracellular Reactive Oxygen Species Generated upon Exposure to Naphthalene

656   Secondary Organic Aerosols, Environ. Sci. Technol. Lett., 7, 171-177, 2020.

657   Liu, Q., Baumgartner, J., Zhang, Y., Liu, Y., Sun, Y., and Zhang, M.: Oxidative potential and inflammatory

658   impacts of source apportioned ambient air pollution in Beijing, Environ. Sci. Technol., 48, 12920-12929,

659   2014.

660   Lloyd, R. V., Hanna, P. M., and Mason, R. P.: The origin of the hydroxyl radical oxygen in the Fenton

661   reaction, Free Radical Biol. Med., 22, 885-888, 1997.

662   Ma, Y., Cheng, Y., Qiu, X., Cao, G., Fang, Y., Wang, J., Zhu, T., Yu, J., and Hu, D.: Sources and oxidative

663   potential of water-soluble humic-like substances (HULIS WS) in fine particulate matter ($PM_{2.5}$) in Beijing,

664   Atmos. Chem. Phys., 18, 5607-5617, 2018.

665   Maenhaut, W., Nava, S., Lucarelli, F., Wang, W., Chi, X., and Kulmala, M.: Chemical composition, impact

666   from biomass burning, and mass closure for $PM_{2.5}$ and PM_{10} aerosols at Hyytiälä, Finland, in summer 2007,

667   X-Ray Spectrom., 40, 168-171, 2011.

668   Molina, C., Toro, R., Manzano, C., Canepari, S., Massimi, L., and Leiva-Guzmán, M. A.: Airborne aerosols

669   and human health: Leapfrogging from mass concentration to oxidative potential, Atmosphere, 11, 917,

670   2020.

671 Möller, D.: Atmospheric hydrogen peroxide: Evidence for aqueous-phase formation from a historic
672 perspective and a one-year measurement campaign, Atmos. Environ., 43, 5923-5936, 2009.

673 Møller, P., Jacobsen, N. R., Folkmann, J. K., Danielsen, P. H., Mikkelsen, L., Hemmingsen, J. G., Vesterdal,
674 L. K., Forchhammer, L., Wallin, H., and Loft, S.: Role of oxidative damage in toxicity of particulates, Free
675 Radic. Res., 44, 1-46, 2010.

676 Mutzel, A., Poulain, L., Berndt, T., Iinuma, Y., Rodigast, M., Böge, O., Richters, S., Spindler, G., Sipilä,
677 M., Jokinen, T., Markku, K., and Hartmut, H.: Highly oxidized multifunctional organic compounds
678 observed in tropospheric particles: A field and laboratory study, Environ. Sci. Technol., 49, 7754-7761,
679 2015.

680 Nel, A.: Air pollution-related illness: effects of particles, Science, 308, 804-806, 2005.

681 Ohyama, M., Otake, T., Adachi, S., Kobayashi, T., and Morinaga, K.: A comparison of the production of
682 reactive oxygen species by suspended particulate matter and diesel exhaust particles with macrophages,
683 Inhal. Toxicol., 19, 157-160, 2007.

684 Page, S. E., Sander, M., Arnold, W. A., and McNeill, K.: Hydroxyl radical formation upon oxidation of
685 reduced humic acids by oxygen in the dark, Environ. Sci. Technol., 46, 1590-1597, 2012.

686 Park, J., Park, E. H., Schauer, J. J., Yi, S.-M., and Heo, J.: Reactive oxygen species (ROS) activity of
687 ambient fine particles ($PM_{2.5}$) measured in Seoul, Korea, Environ. Int., 117, 276-283, 2018.

688 Pöschl, U.: Air Pollution, Oxidative Stress, and Public Health in the Anthropocene, in: Health of People,
689 Health of Planet and Our Responsibility, Springer, Cham, 79-92, 2020.

690 Pöschl, U., and Shiraiwa, M.: Multiphase chemistry at the atmosphere–biosphere interface influencing
691 climate and public health in the anthropocene, Chem. Rev., 115, 4440-4475, 2015.

692 Pye, H. O., D'Ambro, E. L., Lee, B. H., Schobesberger, S., Takeuchi, M., Zhao, Y., Lopez-Hilfiker, F., Liu,
693 J., Shilling, J. E., and Xing, J.: Anthropogenic enhancements to production of highly oxygenated molecules
694 from autoxidation, Proc. Natl. Acad. Sci. U.S.A., 116, 6641-6646, 2019.

695 Qiu, J., Liang, Z., Tonokura, K., Colussi, A. J., and Enami, S.: Stability of Monoterpene-Derived α-
696 Hydroxyalkyl-Hydroperoxides in Aqueous Organic Media: Relevance to the Fate of Hydroperoxides in
697 Aerosol Particle Phases, Environ. Sci. Technol., 54, 3890-3899, 2020.

698 Qu, J., Li, Y., Zhong, W., Gao, P., and Hu, C.: Recent developments in the role of reactive oxygen species
699 in allergic asthma, J. Thorac. Dis., 9, E32, 2017.

700 Rao, X., Zhong, J., Brook, R. D., and Rajagopalan, S.: Effect of particulate matter air pollution on
701 cardiovascular oxidative stress pathways, Antioxid. Redox. Signal., 28, 797-818, 2018.

702 Reinmuth-Selzle, K., Kampf, C. J., Lucas, K., Lang-Yona, N., Fröhlich-Nowoisky, J., Shiraiwa, M., Lakey,
703 P. S., Lai, S., Liu, F., and Kunert, A. T.: Air pollution and climate change effects on allergies in the

anthropocene: abundance, interaction, and modification of allergens and adjuvants, Environ. Sci. Technol., 51, 4119-4141, 2017.

Roldin, P., Ehn, M., Kurtén, T., Olenius, T., Rissanen, M. P., Sarnela, N., Elm, J., Rantala, P., Hao, L., and Hyttinen, N.: The role of highly oxygenated organic molecules in the Boreal aerosol-cloud-climate system, Nat. Commun., 10, 1-15, 2019.

Scheinhardt, S., Müller, K., Spindler, G., and Herrmann, H.: Complexation of trace metals in size-segregated aerosol particles at nine sites in Germany, Atmos. Environ., 74, 102-109, 2013.

Shi, Y., Dai, Y., Liu, Z., Nie, X., Zhao, S., Zhang, C., and Jia, H.: Light-induced variation in environmentally persistent free radicals and the generation of reactive radical species in humic substances, Front. Environ. Sci. Eng., 14, 1-10, 2020.

Shiraiwa, M., Ueda, K., Pozzer, A., Lammel, G., Kampf, C. J., Fushimi, A., Enami, S., Arangio, A. M., Fröhlich-Nowoisky, J., Fujitani, Y., Furuyama, A., Lakey, P. S. J., Lelieveld, J., Lucas, K., Morino, Y., Pöschl, U., Takahama, S., Takami, A., Tong, H., Weber, B., Yoshino, A., and Sato, K.: Aerosol health effects from molecular to global scales, Environ. Sci. Technol., 51, 13545-13567, 2017.

Shrivastava, M., Andreae, M. O., Artaxo, P., Barbosa, H. M., Berg, L. K., Brito, J., Ching, J., Easter, R. C., Fan, J., and Fast, J. D.: Urban pollution greatly enhances formation of natural aerosols over the Amazon rainforest, Nat. Commun., 10, 1046, 2019.

Sies, H., Berndt, C., and Jones, D. P.: Oxidative stress, Annu. Rev. Biochem., 86, 715-748, 2017.

Simic, M., Neta, P., and Hayon, E.: Pulse radiolysis study of alcohols in aqueous solution, J. Phys. Chem., 73, 3794-3800, 1969.

Singh, D. K., and Gupta, T.: Role of transition metals with water soluble organic carbon in the formation of secondary organic aerosol and metallo‐organics in PM_1 sampled during post monsoon and pre-winter time, J. Aerosol Sci., 94, 56-69, 2016.

Su, H., Cheng, Y., and Pöschl, U.: New Multiphase Chemical Processes Influencing Atmospheric Aerosols, Air Quality, and Climate in the Anthropocene, Acc. Chem. Res., 53, 2034-2043, 2020.

Tan, J., Xiang, P., Zhou, X., Duan, J., Ma, Y., He, K., Cheng, Y., Yu, J., and Querol, X.: Chemical characterization of humic-like substances (HULIS) in $PM_{2.5}$ in Lanzhou, China, Sci. Total Environ., 573, 1481-1490, 2016.

Tang, W.-W., Zeng, G.-M., Gong, J.-L., Liang, J., Xu, P., Zhang, C., and Huang, B.-B.: Impact of humic/fulvic acid on the removal of heavy metals from aqueous solutions using nanomaterials: a review, Sci. Total Environ., 468, 1014-1027, 2014.

Tao, W., Su, H., Zheng, G., Wang, J., Wei, C., Liu, L., Ma, N., Li, M., Zhang, Q., and Pöschl, U.: Aerosol pH and chemical regimes of sulfate formation in aerosol water during winter haze in the North China Plain, Atmos. Chem. Phys., 20, 11729-11746, 2020.

738 Tong, H., Arangio, A. M., Lakey, P. S., Berkemeier, T., Liu, F., Kampf, C. J., Brune, W. H., Pöschl, U.,

739 and Shiraiwa, M.: Hydroxyl radicals from secondary organic aerosol decomposition in water, Atmos. Chem.

740 Phys., 16, 1761-1771, 2016a.

741 Tong, H., Kourtchev, I., Pant, P., Keyte, I. J., O'Connor, I. P., Wenger, J. C., Pope, F. D., Harrison, R. M.,

742 and Kalberer, M.: Molecular composition of organic aerosols at urban background and road tunnel sites

743 using ultra-high resolution mass spectrometry, Faraday Discuss., 189, 51-68, 2016b.

744 Tong, H., Lakey, P. S., Arangio, A. M., Socorro, J., Kampf, C. J., Berkemeier, T., Brune, W. H., Pöschl,

745 U., and Shiraiwa, M.: Reactive oxygen species formed in aqueous mixtures of secondary organic aerosols

746 and mineral dust influencing cloud chemistry and public health in the Anthropocene, Faraday Discuss., 200,

747 251-270, 2017.

748 Tong, H., Lakey, P. S., Arangio, A. M., Socorro, J., Shen, F., Lucas, K., Brune, W. H., Pöschl, U., and

749 Shiraiwa, M.: Reactive oxygen species formed by secondary organic aerosols in water and surrogate lung

750 fluid, Environ. Sci. Technol., 52, 11642-11651, 2018.

751 Tong, H., Zhang, Y., Filippi, A., Wang, T., Li, C., Liu, F., Leppla, D., Kourtchev, I., Wang, K., Keskinen,

752 H.-M., Levula, J. T., Arangio, A. M., Shen, F., Ditas, F., Martin, S. T., Artaxo, P., Godoi, R. H. M.,

753 Yamamoto, C. I., Souza, R. A. F. d., Huang, R.-J., Berkemeier, T., Wang, Y., Su, H., Cheng, Y., Pope, F.

754 D., Fu, P., Yao, M., Pöhlker, C., Petäjä, T., Kulmala, M., Andreae, M. O., Shiraiwa, M., Pöschl, U.,

755 Hoffmann, T., and Kalberer, M.: Radical Formation by Fine Particulate Matter Associated with Highly

756 Oxygenated Molecules, Environ. Sci. Technol., 53, 12506-12518, 2019.

757 Tröstl, J., Chuang, W. K., Gordon, H., Heinritzi, M., Yan, C., Molteni, U., Ahlm, L., Frege, C., Bianchi, F.,

758 and Wagner, R.: The role of low-volatility organic compounds in initial particle growth in the atmosphere,

759 Nature, 533, 527-531, 2016.

760 Tseitlin, M., Eaton, S. S., and Eaton, G. R.: Uncertainty analysis for absorption and first‐derivative

761 electron paramagnetic resonance spectra, Concepts Magn. Reson., Part A, 40, 295-305, 2012.

762 Valavanidis, A., Salika, A., and Theodoropoulou, A.: Generation of hydroxyl radicals by urban suspended

763 particulate air matter. The role of iron ions, Atmos. Environ., 34, 2379-2386, 2000.

764 Valavanidis, A., Fiotakis, K., Bakeas, E., and Vlahogianni, T.: Electron paramagnetic resonance study of

765 the generation of reactive oxygen species catalysed by transition metals and quinoid redox cycling by

766 inhalable ambient particulate matter, Redox. Rep., 10, 37-51, 2005.

767 Vejerano, E. P., Rao, G., Khachatryan, L., Cormier, S. A., and Lomnicki, S.: Environmentally persistent

768 free radicals: Insights on a new class of pollutants, Environ. Sci. Technol., 52, 2468-2481, 2018.

769 Verma, V., Fang, T., Guo, H., King, L., Bates, J., Peltier, R., Edgerton, E., Russell, A., and Weber, R.:

770 Reactive oxygen species associated with water-soluble $PM_{2.5}$ in the southeastern United States:

771 spatiotemporal trends and source apportionment, Atmos. Chem. Phys., 14, 12915-12930, 2014.

772 Verma, V., Fang, T., Xu, L., Peltier, R. E., Russell, A. G., Ng, N. L., and Weber, R. J.: Organic aerosols

773 associated with the generation of reactive oxygen species (ROS) by water-soluble $PM_{2.5}$, Environ. Sci.

774 Technol., 49, 4646-4656, 2015.

775 Wang, C., Wang, Z., Peng, A., Hou, J., and Xin, W.: Interaction between fulvic acids of different origins

776 and active oxygen radicals, Sci. China C Life Sci., 39, 267-275, 1996.

777 Wang, K., Zhang, Y., Huang, R.-J., Cao, J., and Hoffmann, T.: UHPLC-Orbitrap mass spectrometric

778 characterization of organic aerosol from a central European city (Mainz, Germany) and a Chinese megacity

779 (Beijing), Atmos. Environ., 189, 22-29, 2018a.

780 Wang, K., Zhang, Y., Huang, R.-J., Wang, M., Ni, H., Kampf, C. J., Cheng, Y., Bilde, M., Glasius, M., and

781 Hoffmann, T.: Molecular characterization and source identification of atmospheric particulate

782 organosulfates using ultrahigh resolution mass spectrometry, Environ. Sci. Technol., 53, 6192-6202, 2019.

783 Wang, N., Miller, C. J., Wang, P., and Waite, T. D.: Quantitative determination of trace hydrogen peroxide

784 in the presence of sulfide using the Amplex Red/horseradish peroxidase assay, Anal. Chim. Acta, 963, 61-

785 67, 2017.

786 Wang, S., Ye, J., Soong, R., Wu, B., Yu, L., Simpson, A. J., and Chan, A. W.: Relationship between

787 chemical composition and oxidative potential of secondary organic aerosol from polycyclic aromatic

788 hydrocarbons, Atmos. Chem. Phys., 18, 3987-4003, 2018b.

789 Wang, W., Liu, M., Wang, T., Song, Y., Zhou, L., Cao, J., Hu, J., Tang, G., Chen, Z., and Li, Z.: Sulfate

790 formation is dominated by manganese-catalyzed oxidation of SO 2 on aerosol surfaces during haze events,

791 Nat. Commun., 12, 1-10, 2021.

792 Wang, Y., Arellanes, C., Curtis, D. B., and Paulson, S. E.: Probing the source of hydrogen peroxide

793 associated with coarse mode aerosol particles in Southern California, Environ. Sci. Technol., 44, 4070-

794 4075, 2010.

795 Wang, Y., Hopke, P. K., Sun, L., Chalupa, D. C., and Utell, M. J.: Laboratory and field testing of an

796 automated atmospheric particle-bound reactive oxygen species sampling-analysis system, J. Toxicol., 2011,

797 419476, 2011a.

798 Wang, Y., Kim, H., and Paulson, S. E.: Hydrogen peroxide generation from α-and β-pinene and toluene

799 secondary organic aerosols, Atmos. Environ., 45, 3149-3156, 2011b.

800 Wang, Y., Arellanes, C., and Paulson, S. E.: Hydrogen peroxide associated with ambient fine-mode, diesel,

801 and biodiesel aerosol particles in Southern California, Aerosol Sci. Technol., 46, 394-402, 2012.

802 Wang, Y., Hu, M., Guo, S., Wang, Y., Zheng, J., Yang, Y., Zhu, W., Tang, R., Li, X., and Liu, Y.: The

803 secondary formation of organosulfates under interactions between biogenic emissions and anthropogenic

804 pollutants in summer in Beijing, Atmos. Chem. Phys., 18, 10693-10713, 2018c.

805   Wei, J., Yu, H., Wang, Y., and Verma, V.: Complexation of Iron and Copper in Ambient Particulate Matter

806   and Its Effect on the Oxidative Potential Measured in a Surrogate Lung Fluid, Environ. Sci. Technol., 53,

807   1661-1671, 2019.

808   Wei, J., Fang, T., Wong, C., Lakey, P. S., Nizkorodov, S. A., and Shiraiwa, M.: Superoxide Formation from

809   Aqueous Reactions of Biogenic Secondary Organic Aerosols, Environ. Sci. Technol., 55, 260-270, 2021.

810   Win, M. S., Tian, Z., Zhao, H., Xiao, K., Peng, J., Shang, Y., Wu, M., Xiu, G., Lu, S., and Yonemochi, S.:

811   Atmospheric HULIS and its ability to mediate the reactive oxygen species (ROS): A review, J. Environ.

812   Sci., 71, 13-31, 2018.

813   Xia, T., Korge, P., Weiss, J. N., Li, N., Venkatesen, M. I., Sioutas, C., and Nel, A.: Quinones and aromatic

814   chemical compounds in particulate matter induce mitochondrial dysfunction: implications for ultrafine

815   particle toxicity, Environ. Health Perspect., 112, 1347-1358, 2004.

816   Xiong, Q., Yu, H., Wang, R., Wei, J., and Verma, V.: Rethinking dithiothreitol-based particulate matter

817   oxidative potential: measuring dithiothreitol consumption versus reactive oxygen species generation,

818   Environ. Sci. Technol., 51, 6507-6514, 2017.

819   Xu, L., Guo, H., Boyd, C. M., Klein, M., Bougiatioti, A., Cerully, K. M., Hite, J. R., Isaacman-VanWertz,

820   G., Kreisberg, N. M., and Knote, C.: Effects of anthropogenic emissions on aerosol formation from isoprene

821   and monoterpenes in the southeastern United States, Proc. Natl. Acad. Sci. U.S.A., 112, 37-42, 2015.

822   Yan, D., Cui, H., Zhu, W., Talbot, A., Zhang, L. G., Sherman, J. H., and Keidar, M.: The strong cell-based

823   hydrogen peroxide generation triggered by cold atmospheric plasma, Sci. Rep., 7, 1-9, 2017.

824   Yang, R., Su, H., Qu, S., and Wang, X.: Capacity of humic substances to complex with iron at different

825   salinities in the Yangtze River estuary and East China Sea, Sci. Rep., 7, 1381, 2017.

826   Yassine, M. M., Harir, M., Dabek‑Zlotorzynska, E., and Schmitt‑Kopplin, P.: Structural characterization

827   of organic aerosol using Fourier transform ion cyclotron resonance mass spectrometry: aromaticity

828   equivalent approach, Rapid Commun. Mass Spectrom., 28, 2445-2454, 2014.

829   Yu, H., Wei, J., Cheng, Y., Subedi, K., and Verma, V.: Synergistic and antagonistic interactions among the

830   particulate matter components in generating reactive oxygen species based on the dithiothreitol assay,

831   Environ. Sci. Technol., 52, 2261-2270, 2018.

832   Yun, X., Shen, G., Shen, H., Meng, W., Chen, Y., Xu, H., Ren, Y., Zhong, Q., Du, W., and Ma, J.:

833   Residential solid fuel emissions contribute significantly to air pollution and associated health impacts in

834   China, Sci. Adv., 6, eaba7621, 2020.

835   Zhang, Y., and Tao, S.: Global atmospheric emission inventory of polycyclic aromatic hydrocarbons (PAHs)

836   for 2004, Atmos. Environ., 43, 812-819, 2009.

837 Zhao, H., Joseph, J., Zhang, H., Karoui, H., and Kalyanaraman, B.: Synthesis and biochemical applications

838 of a solid cyclic nitrone spin trap: a relatively superior trap for detecting superoxide anions and glutathiyl

839 radicals, Free Radic. Biol. Med., 31, 599-606, 2001.

840 Zheng, G., He, K., Duan, F., Cheng, Y., and Ma, Y.: Measurement of humic-like substances in aerosols: A

841 review, Environ. Pollut., 181, 301-314, 2013.

842 Zheng, G., Su, H., Wang, S., Andreae, M. O., Pöschl, U., and Cheng, Y.: Multiphase buffer theory explains

843 contrasts in atmospheric aerosol acidity, Science, 369, 1374-1377, 2020.

844 Zhou, J., Zotter, P., Bruns, E. A., Stefenelli, G., Bhattu, D., Brown, S., Bertrand, A., Marchand, N.,

845 Lamkaddam, H., and Slowik, J. G.: Particle-bound reactive oxygen species (PB-ROS) emissions and

846 formation pathways in residential wood smoke under different combustion and aging conditions, Atmos.

847 Chem. Phys., 18, 6985-7000, 2018.

848 Zuo, Y., and Hoigne, J.: Formation of hydrogen peroxide and depletion of oxalic acid in atmospheric water

849 by photolysis of iron(III)-oxalato complexes, Environ. Sci. Technol., 26, 1014-1022, 1992.

850 Zuo, Y., and Deng, Y.: Iron (II)-catalyzed photochemical decomposition of oxalic acid and generation of

851 H_2O_2 in atmospheric liquid phases, Chemosphere, 35, 2051-2058, 1997.

852

853 *Data availability*

854 The dataset for this paper is available upon request from the corresponding author (h.tong@mpic.de).

855 *Supporting Information*

856 Supporting material consists of seven figures and five tables.

857 *Author contributions*

858 HT and UP designed the esperiment and wrote up the original draft together with FL. CX, SY, and HK

859 involved in the collection of ambient particles. HT, FL, AF, and YZ participated in laboratory

860 measurements and data analysis. All other co-authors participated in results discussion and manuscript

861 editing.

862 *AUTHOR INFORMATION*

863 *Corresponding Author*

864 *Haijie Tong*

865 Phone: (+852) 2766-6025

866 E-mail: h.tong@mpic.de; haijie.tong@polyu.edu.hk.

867 *ORCID*:

868 Haijie Tong: 0000-0001-9887-7836

869 Maosheng Yao: 0000-0002-1442-8054

870 Thomas Berkemeier: 0000-0001-6390-6465

871 Manabu Shiraiwa: 0000-0003-2532-5373

872 Ulrich Pöschl: 0000-0003-1412-35570000-0001-9887-7836

873 *Competing interests*

874 The authors declare no competing financial interest.

875 *Acknowledgements*

876   This work was funded by the Max Planck Society, ACTRIS, ECAC, the Finnish Centre of Excellence under

877   Academy of Finland (projects no. 307331 and 272041), and PolyU (P0036313). Siegfried Herrmann and

878   Steve Galer from Climate Geochemistry Department of Max Planck Institute for Chemistry are gratefully

879   acknowledged for ICP-MS analysis. Technical staffs at SMEARII station are acknowledged for the

880   impactor maintenance. MS acknowledges funding from the National Science Foundation (CHE-1808125).
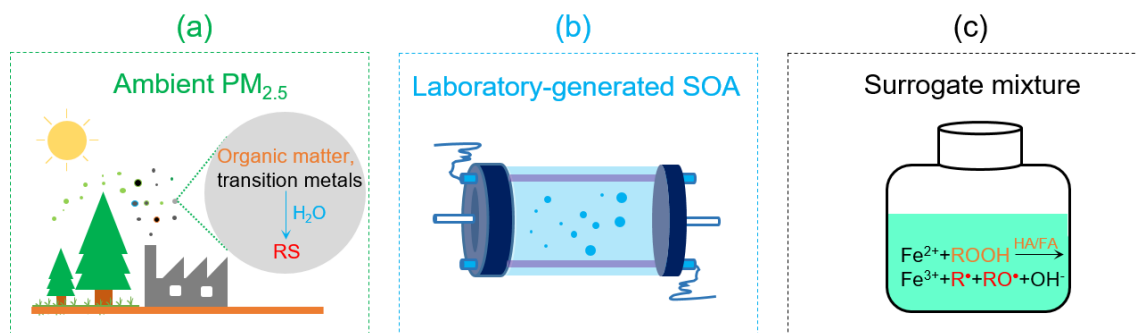
Figure 1. Schematic illustration of research approach and comparison of aqueous-phase reactive species (RS) formed in aqueous extracts of ambient fine particulate matter ($PM_{2.5}$), and laboratory generated secondary organic aerosols (SOA), and surrogate mixtures. ROOH: organic hydroperoxide. HA: humic acid. FA: fulvic acid. $R^•$ and $RO^•$: C- and O-centered organic radicals, respectively.
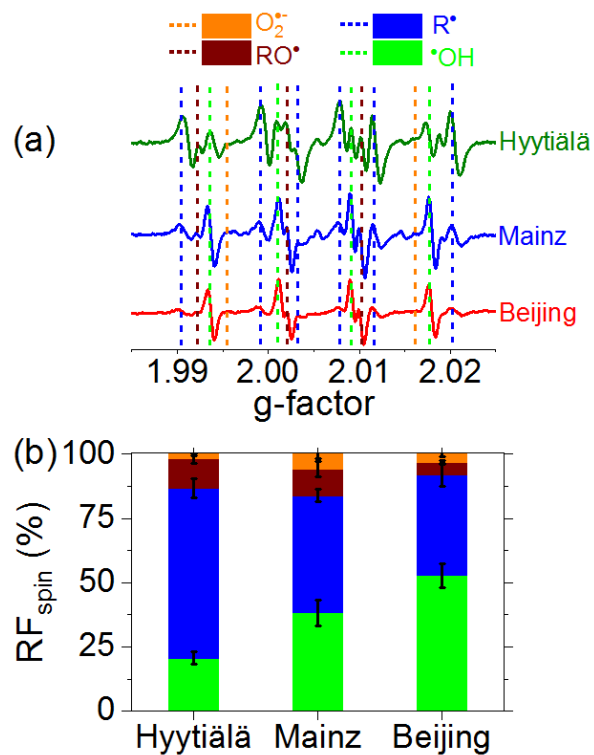
Figure 2. (a) Electron paramagnetic resonance (EPR) spectra and (b) relative fraction of unpaired electrons (RF$_{spin}$) attributed to different types of radicals formed in aqueous extracts of ambient PM$_{2.5}$ from Hyytiälä, Mainz, and Beijing. Dotted vertical lines in (a) indicate peak positions of different radical adducts. The spectra intensity in (a), RF$_{spin}$ values and error bars in (b) represent arithmetic mean values and standard error (6-13 samples per location).

892
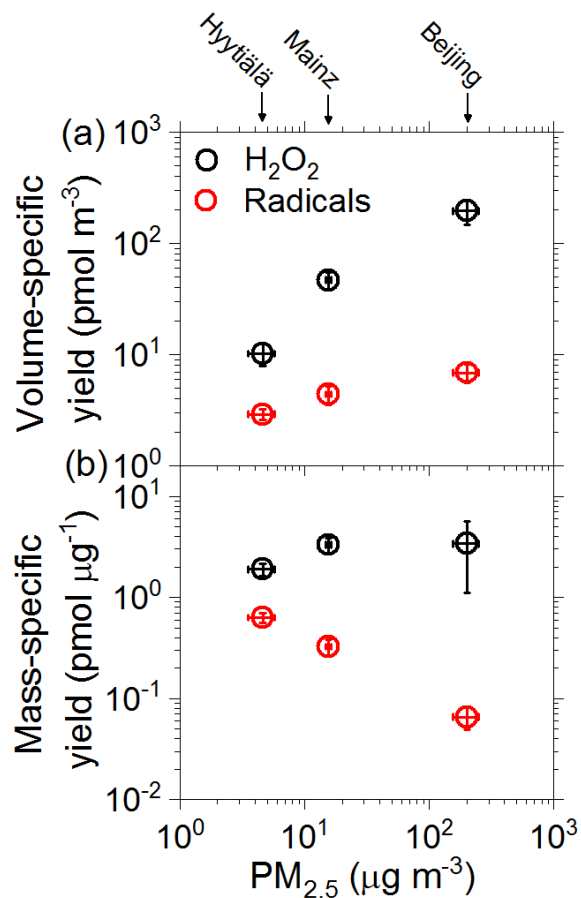
Figure 3. (a) Air sample volume-specific yields and (b) mass-specific yields of aqueous-phase radicals (○)

and H_2O_2 (○) formed in aqueous extracts of ambient $PM_{2.5}$ from Hyytiälä, Mainz, and Beijing. plotted

against $PM_{2.5}$ mass concentration. The error bars represent standard errors of the mean (4-12 samples per

location).

897
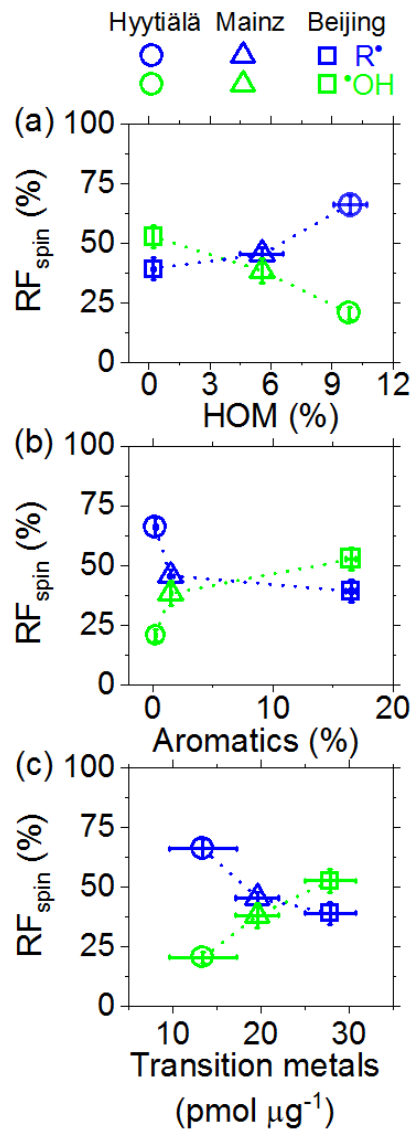
Figure 4. Relative fraction (RF_{spin}) of aqueous-phase C-centered (R$^\bullet$) and $^\bullet$OH radicals plotted against the relative abundance of (a) highly oxygenated organic molecules (HOM), (b) aromatics, and (c) water-soluble transition metals in ambient PM$_{2.5}$ from Hyytiälä, Mainz, and Beijing. The relative abundances of HOM and aromatics in (a-b) represent the sum chromatographic area of HOM or aromatics divided by the sum chromatographic area of all assigned organic compounds. The abundances of HOM in (a) were adopted from a recent companion study (Tong et al., 2019). The error bars represent standard errors of the mean (4 to 12 samples per location). The dashed lines are to guide the eye.

905
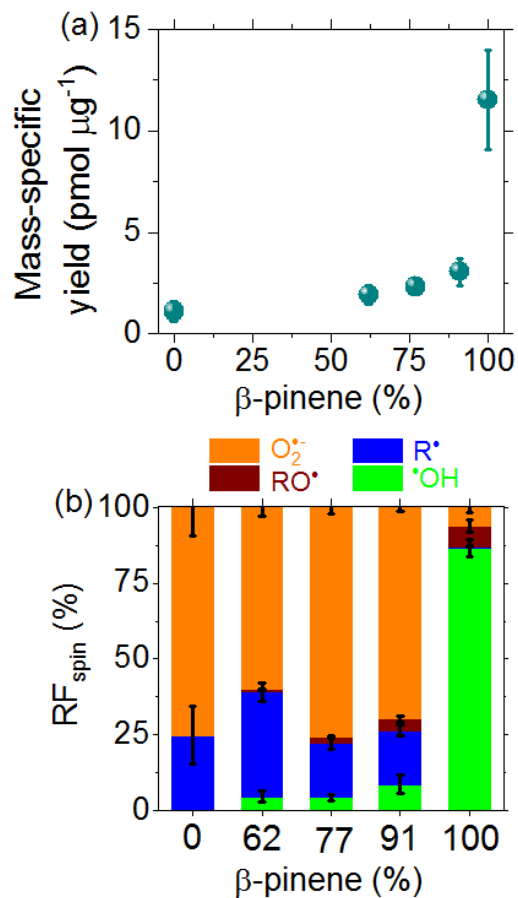
Figure 5. (a) Mass-specific yields and (b) relative fractions (RF$_{spin}$) of different types of radicals formed upon aqueous extraction of laboratory-generated SOA from precursor mixtures of β-pinene and naphthalene plotted against the mass fraction of β-pinene (%) in the precursor mixture. The error bars represent standard errors (4-6 samples per data point).
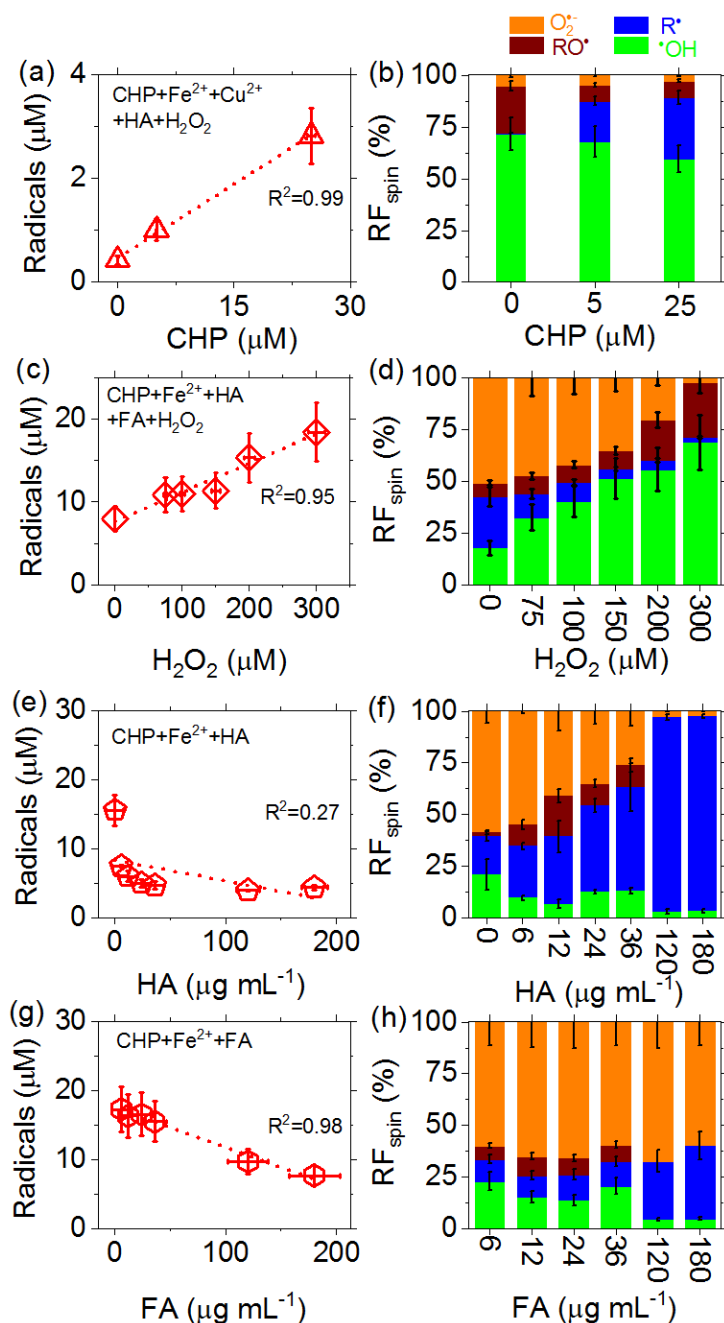
Figure 6. (a, c, e, g) Total concentrations and (b, d, f, h) relative fractions (RF_{spin}) of different types of radicals (spins) observed in aqueous mixtures of Fe^{2+}, Cu^{2+}, humic acid (HA), fulvic acid (FA), cumene hydroperoxide (CHP), and H_2O_2, serving as surrogate species for redox-active components of $PM_{2.5}$. (a, b): 0-25 µM CHP, 43 µM Fe^{2+}, 3 µM Cu^{2+}, 4 µg mL^{-1} HA, 7 µM H_2O_2 (CHP+Fe^{2+}+Cu^{2+}+HA+H_2O_2). (c, d): CHP: 100 µM. Fe^{2+}: 300 µM. HA: 100 µg mL^{-1}. FA: 80 µg mL^{-1}. H_2O_2: 0-300 µM. (e, f): 100 µM CHP, 300 µM Fe^{2+}, 0-180 µg mL^{-1} HA (CHP+Fe^{2+}+HA). (g, h): 100 µM CHP, 300 µM Fe^{2+}, 6-180 µg mL^{-1} FA (CHP+Fe^{2+}+FA). The error bars represent the uncertainties of EPR signal integration (y-axis) and solute concentration (x-axis), respectively.